

pyUserCalc: A revised Jupyter notebook calculator for uranium-series disequilibria in basalts

Lynne J. Elkins¹, Marc Spiegelman²

¹University of Nebraska-Lincoln, Lincoln, NE, USA

²Lamont-Doherty Earth Observatory of Columbia University, Palisades, NY, USA

Key Points:

- Cloud-based Jupyter notebook presents an open source, reproducible tool for modeling U-series in basalts
- Equilibrium and pure disequilibrium porous flow U-series models with 1D conservation of mass
- Scaled porous flow model introduces incomplete equilibrium scenario with reaction rate limitations

Corresponding author: Lynne J. Elkins, lelkins@unl.edu

Abstract

Meaningful analysis of uranium-series isotopic disequilibria in basaltic lavas relies on the use of complex forward numerical models like dynamic melting McKenzie (1985) and equilibrium porous flow Spiegelman & Elliott (1993). Historically, such models have either been solved analytically for simplified scenarios, such as constant melting rate or constant solid/melt trace element partitioning throughout the melting process, or have relied on incremental or numerical calculators with limited power to solve problems and/or restricted availability. The most public numerical solution to reactive porous flow, UserCalc Spiegelman (2000) was maintained on a private institutional server for nearly two decades, but that approach has been unsustainable in light of modern security concerns. Here we present a more long-lasting solution to the problems of availability, model sophistication and flexibility, and long-term access in the form of a cloud-hosted, publicly available Jupyter notebook. Similar to UserCalc, the new notebook calculates U-series disequilibria during time-dependent, equilibrium partial melting in a one-dimensional porous flow regime where mass is conserved. In addition, we also provide a new disequilibrium transport model which has the same melt transport model as UserCalc, but approximates rate-limited diffusive exchange of nuclides between solid and melt using linear kinetics. The degree of disequilibrium during transport is controlled by a Damköhler number, allowing the full spectrum of equilibration models from complete fractional melting ($Da = 0$) to equilibrium transport ($Da = \infty$).

Access this manuscript as a static HTML or downloadable PDF file on the Earth and Space Science journal website here: Elkins & Spiegelman (2021).

0.1 Introduction

Continuous forward melting models are necessary to interpret the origins of empirically-measured U-series isotopic disequilibria in basaltic lavas, but the limited and unreliable availability of reproducible tools for making such calculations remains a persistent problem for geochemists. To date, a number of models have been developed for this task, including classical dynamic melting after McKenzie (1985) and the reactive porous flow model of Spiegelman & Elliott (1993). There have since been numerous approaches to using both the dynamic and porous flow models that range from simplified analytical solutions Sims et al. (1999); Zou & Zindler (2000) to incremental dynamic melting calculators Stracke et al. (2003), two-porosity calculators Jull et al. (2002); Lundstrom et al. (2000); Sims et al. (2002), and one-dimensional numerical solutions to reactive porous flow Spiegelman (2000) and dynamic melting Bourdon et al. (2005); Elkins et al. (2019). Unfortunately, some of the approaches published since 1990 lacked publicly available tools that would permit others to directly apply the authors' methods, and while the more simplified and incremental approaches remain appropriate for asking and approaching some questions, they are insufficient for other applications that require more complex approaches Elkins et al. (2019). Other tools like UserCalc that were available to public users Spiegelman (2000) were limited in application and have since become unavailable.

In light of the need for more broadly accessible and flexible solutions to U-series disequilibrium problems in partial melting, here we present a cloud-server hosted, publicly available numerical calculator for one-dimensional, decompression partial melting. The tool is provided in a Jupyter notebook with importable Python code and can be accessed from a web browser. Users will be able to access and use the tool using a free cloud server account, or on their own computer given any standard Python distribution. As shown below, the notebook is structured to permit the user to select one of two primary model versions, either classical reactive porous flow after Spiegelman & Elliott (1993) and Spiegelman (2000), or a new disequilibrium transport model, developed after the appendix formulas of Spiegelman & Elliott (1993). The new model ranges from pure disequilibrium porous flow transport (i.e., the mass-conserved equivalent of true fractional

melting over time) to a “scaled” disequilibrium scenario, where the degree of chemical equilibrium that is reached is determined by the relationship between the rate of chemical reaction and the solid decompression rate (which is, in turn, related to the overall melting rate), in the form of a Damköhler number.

This scaled disequilibrium model resembles the classic dynamic melting model of McKenzie (1985), with the caveat that ours is the first U-series melting model developed for near-fractional, disequilibrium transport where mass is also conserved within a one-dimensional melting regime. That is, rather than controlling the quantity of melt that remains in equilibrium with the solid using a fixed residual porosity, the melt porosity is controlled by Darcy’s Law and mass conservation constraints after Spiegelman & Elliott (1993), and the “near-fractional” scenario is simulated using the reaction rate of the migrating liquid with the upwelling solid matrix.

0.2 Calculating U-series in basalts during mass-conserved, one-dimensional porous flow

0.2.1 Solving for equilibrium transport

Here we consider several forward melting models that calculate the concentrations and activities of U-series isotopes (^{238}U , ^{230}Th , ^{226}Ra , ^{235}U , and ^{231}Pa) during partial melting and melt transport due to adiabatic mantle decompression. Following Spiegelman & Elliott (1993), we start with conservation of mass equations for the concentration of a nuclide i , assuming chemical equilibrium between melt and solid:

$$\begin{aligned} \frac{\partial}{\partial t}[\rho_f\phi + \rho_s(1-\phi)D_i]c_i^f + \nabla \cdot [\rho_f\phi v + \rho_s(1-\phi)D_iV]c_i^f \\ = \lambda_{i-1}[\rho_f\phi + \rho_s(1-\phi)D_{i-1}]c_{i-1}^f - \lambda_i[\rho_f\phi + \rho_s(1-\phi)D_i]c_i^f \end{aligned} \quad (1)$$

where t is time, c_i^f is the concentration of nuclide i in the melt, D_i is the bulk solid/liquid partition coefficient for nuclide i , ρ_f is the density of the fluid and ρ_s is the density of the solid, ϕ is the porosity (local volume fraction of melt), v is the velocity of the melt and V the velocity of the solid in three dimensions, λ_i is the decay constant of nuclide i , and $(i-1)$ indicates the radioactive parent of nuclide i (see Table 1). Equation (1) states that the change in total mass of nuclide i in both the melt and the solid is controlled by the divergence of the mass flux transported by both phases and by the radioactive decay of both parent and daughter nuclides (i.e., the right hand side of the equation above).

The equilibrium model of Spiegelman & Elliott (1993) assumes that complete chemical equilibrium is maintained between the migrating partial melt and the solid rock matrix along a decompressing one-dimensional column. To close the equations, they assume that melt transport is described by a simplified form of Darcy’s Law for permeable flow through the solid matrix. In one dimension, for a steady-state upwelling column of melting mantle rocks, they defined the one-dimensional melt and solid velocities (w and W , respectively), and expressed the melt and solid fluxes as functions of height (z) in terms of a constant melting rate Γ_0 :

$$\rho_f\phi w = \Gamma_0 z \quad (2)$$

$$\rho_s(1-\phi)W = \rho_s W_0 - \Gamma_0 z \quad (3)$$

where W_0 is the solid mantle upwelling rate, and Γ_0 is equivalent to $\rho_s W_0 F_{max}$ divided by the column height h for a maximum degree of melting F_{max} .

Table 1. List of variables used in this study.

Variable	Definition
c_i^f	Concentration of nuclide i in the liquid
c_i^s	Concentration of nuclide i in the solid
U_i^f	Natural log of the concentration of nuclide i in the liquid relative to its initial concentration
U_i^s	Natural log of the concentration of nuclide i in the solid relative to its initial concentration
U_i^{stable}	Stable element component of U_i^f
U_i^{rad}	Radiogenic component of U_i^f
a_i	Activity of nuclide i
a_i^0	Initial activity of nuclide i
z	Height in a one-dimensional melting column
h	Total height of the melting column
ζ	$= z/h$, Dimensionless fractional height in scaled one-dimensional melting column
D_i	Bulk solid/liquid partition coefficient for nuclide i
D_i^0	Initial bulk solid/liquid partition coefficient for nuclide i
ρ_f	Density of the liquid
ρ_s	Density of the solid
ϕ	Porosity (volume fraction of liquid present)
ϕ_0	Maximum or reference porosity
V	Solid velocity
v	Liquid velocity
W	One-dimensional solid velocity
w	One-dimensional liquid velocity
W_0	Solid mantle upwelling velocity
λ_i	Decay constant for nuclide i
λ_i'	$= \lambda_i h/W_0$, Decay constant for nuclide i scaled by solid transport time
Γ	Melting rate
Γ_0	Constant melting rate
F_{max}	Maximum degree of melting
w_{eff}^i	Effective liquid velocity of nuclide i
R_i^{i-1}	Ingrowth factor
α_i^0	Initial degree of secular disequilibrium in the unmelted solid
k	Permeability
K_r	Relative permeability factor
n	Permeability exponent
A_d	Permeability calibration function
\Re	Reactivity rate factor
d	Diffusion/Reaction length scale (e.g., grain-size)
Da	Damköhler number

Assuming an initial condition of secular equilibrium, where the initial activities $\lambda_i c_{i,0}^f D_i$ are equivalent for parent and daughter nuclides, they derived a system of differential equations for the concentration c_i^f in any decay chain, which can be solved numerically using equation (10) from Spiegelman & Elliott (1993):

$$\frac{dc_i'}{d\zeta} = c_i' \frac{(D_i - 1)F_{max}}{D_i + (1 - D_i)F_{max}\zeta} + \lambda_i h \left[\frac{D_i[D_{i-1} + (1 - D_{i-1})F_{max}\zeta]}{D_{i-1}[D_i + (1 - D_i)F_{max}\zeta]} \frac{c_{i-1}'}{w_{eff}^{i-1}} - \frac{c_i'}{w_{eff}^i} \right] \quad (4)$$

where c_i' is the scaled melt concentration ($= c_i^f / c_{i,0}^f$), ζ is the dimensionless fractional height in the scaled column, equal to 0 at the base and 1 at the top, and

$$w_{eff}^i = \frac{\rho_f \phi w + \rho_s (1 - \phi) D_i W}{\rho_f \phi + \rho_s (1 - \phi) D_i} \quad (5)$$

is the effective velocity for element i .

In their appendix, Spiegelman & Elliott (1993) developed the more general (and, arguably, realistic) form where Γ and D_i are functions of height z . The UserCalc model of Spiegelman (2000) then formulated a one-dimensional numerical integration for the concentrations of selected U-series isotopes in continuously produced partial melts with height z , after the equilibrium formulas above. The concentration expression derived by Spiegelman (2000) for the equilibrium scenario (formula 6 in Spiegelman (2000)) is:

$$\frac{dc_i^f}{dz} = \frac{-c_i^f(z)}{F(z) + (1 - F(z))D_i(z)} \frac{d}{dz} [F(z) + (1 - F(z))D_i(z)] + \frac{\lambda_{i-1} \overline{\rho D_{i-1}} c_{i-1}^f(z) - \lambda_i \overline{\rho D_i} c_i^f(z)}{\rho_s W_0 [F(z) + (1 - F(z))D_i(z)]} \quad (6)$$

where F is the degree of melting. Spiegelman (2000) further observed that solving for the natural log of the concentrations normalized to the initial concentration of i , U_i , rather than the concentrations themselves, is more accurate, particularly for highly incompatible elements (formulas 7-9 in that reference). This is because log concentrations change linearly during melting, rather than exponentially, and are more numerically stable to calculate.

$$U_i^f = \ln \left(\frac{c_i^f}{c_{i,0}^f} \right) \quad (7)$$

$$\frac{dU_i^f}{dz} = \frac{1}{c_i^f(z)} \frac{dc_i^f}{dz} \quad (8)$$

$$\frac{dU_i^f}{dz} = \frac{-1}{F(z) + (1 - F(z))D_i(z)} \frac{d}{dz} [F(z) + (1 - F(z))D_i(z)] + \frac{\lambda_i}{w_{eff}^i} [R_i^{i-1} \exp[U_{i-1}^f(z) - U_i^f(z)] - 1] \quad (9)$$

For the formulas above, Spiegelman (2000) defined a series of variables that allow for simpler integration formulas and aid in efficient solution of the model, namely

$$\overline{\rho D_i} = \rho_f \phi + \rho_s (1 - \phi) D_i(z), \quad (10)$$

$$\overline{F} = F(z) + (1 - F(z))D_i(z), \quad (11)$$

$$R_i^{i-1} = \alpha_i^0 \frac{D_i^0}{D_{i-1}^0} \frac{\overline{\rho D_{i-1}}}{\overline{\rho D_i}}, \quad (12)$$

$$\alpha_i^0 = \frac{\lambda_{i-1} c_{(i-1),0}^s}{\lambda_i c_{i,0}^s}, \quad (13)$$

124 and substituting from the formulas above

$$w_{eff}^i = \frac{\rho_s W_0 \overline{F}}{\overline{\rho D_i}}. \quad (14)$$

125 where D_i^0 is the initial bulk solid/melt partition coefficient for element i , R_i^{i-1} is
126 the ingrowth factor, and α_i^0 is the initial degree of secular disequilibrium for nuclide i
127 in the unmelted solid.

128 $U_i(z) = \ln(c_f(z)/c_f^0)$, the log of the total concentration of nuclide i in the melt,
129 can then be decomposed into

$$U_i(z) = U_i^{stable}(z) + U_i^{rad}(z) \quad (15)$$

130 where

$$U_i^{stable}(z) = \ln \left[\frac{D_i^0}{\overline{F D_i}(z)} \right] \quad (16)$$

131 is the log concentration of a stable nuclide with the same partition coefficients, and
132 $U_i^{rad}(z)$ is the radiogenic ingrowth component. An alternate way of writing the radio-
133 genic ingrowth component of equation (9) of Spiegelman (2000) is:

$$\frac{dU_i^{rad}}{d\zeta} = \lambda'_i \frac{\overline{\rho D_i}}{\overline{F D_i}} [R_i^{i-1} \exp[U_{i-1}(\zeta) - U_i(\zeta)] - 1] \quad (17)$$

134 where

$$\lambda'_i = \frac{h \lambda_i}{W_0} \quad (18)$$

135 is the decay constant of nuclide i , scaled by the solid transport time (h/W_0) across
136 a layer of total height h . Note equation (17) is solved over a column of dimensionless height
137 1 where $\zeta \in [0, 1]$.

138 Using these equations, the UserCalc reactive porous flow calculator accepted user
139 inputs for both $F(z)$ and $D_i(z)$. The method further uses a formula for the melt poros-
140 ity ($\phi(z)$) based on a Darcy's Law expression with a relative permeability factor (for-
141 mula 20 from Spiegelman (2000)):

$$K_r(z) A_d \phi^n (1 - \phi)^2 + \phi [1 + F(z) (\frac{\rho_s}{\rho_f} - 1)] - \frac{\rho_s}{\rho_f} F(z) = 0 \quad (19)$$

where $K_r(z)$ is the relative permeability with height z , A_d is a permeability calibration function, and n is the permeability exponent. The permeability exponent for a tube-shaped fluid network is expected to be $n = 2$, while for a sheet-shaped network it is $n = 3$; recent measurements of the permeabilities of experimental magmatic melt networks suggest realistic magma migration occurs in a manner intermediate between these two scenarios, with $n = 2.6$ Miller et al. (2014). The relative permeability K_r is calculated with respect to the permeability at the top of the column, i.e. depth $z = z_{final}$:

$$K_r(z) = \frac{k(z)}{k(z_{final})} \quad (20)$$

and allows for locally enhanced flow (e.g., mimicking the effects of a relatively low viscosity fluid).

Our model implementation reproduces and builds on the prior efforts summarized above, using a readily accessible computer language (Python) and web application (Jupyter notebooks).

0.2.2 Solving for complete disequilibrium transport

We further present a calculation tool that solves a similar set of equations for pure chemical disequilibrium transport during one-dimensional decompression melting. This model assumes that the solid produces an instantaneous fractional melt in local equilibrium with the solid; however, the melt is not allowed to back-react with the solid during transport, as it would in the equilibrium model above. In the limiting condition defined by stable trace elements (i.e., without radioactive decay), the model reduces to the calculation for an accumulated fractional melt. The model solves for the concentration of each nuclide i in the solid (s) and liquid (f) using equations (26) and (27) of Spiegelman & Elliott (1993):

$$\frac{dc_i^s}{dz} = \frac{c_i^s(z)(1 - \frac{1}{D_i(z)})}{1 - F(z)} \frac{dF}{dz} + \frac{1 - \phi}{W_0(1 - F(z))} [\lambda_{i-1}c_{i-1}^s(z) - \lambda_i c_i^s(z)] \quad (21)$$

$$\frac{dc_i^f}{dz} = \frac{\frac{c_i^s(z)}{D_i(z)} - c_i^f(z)}{F(z)} \frac{dF}{dz} + \frac{\rho_f \phi}{\rho_s W_0 F(z)} [\lambda_{i-1}c_{i-1}^f(z) - \lambda_i c_i^f(z)] \quad (22)$$

which maintain conservation of mass for both fluid and solid individually, and do not assume chemical equilibration between the two phases. As above, the equations depend on $F(z)$ and $D_i(z)$, i.e. melt fractions and bulk rock partition coefficients that can vary with depth.

As above, the solid and fluid concentration equations are rewritten in terms of the logs of the concentrations:

$$U_i^s(z) = \ln \left(\frac{c_i^s(z)}{c_{i,0}^s} \right), \quad U_i^f(z) = \ln \left(\frac{c_i^f(z)}{c_{i,0}^f} \right) \quad (23)$$

and thus

$$\frac{dU_i}{dz} = \frac{1}{c_i(z)} \frac{dc_i}{dz} \quad (24)$$

We assume that initial $c_{i,0}^s = D_{i,0} c_{i,0}^f$. As above, the log concentration equations can be broken into stable and radiogenic components, where the stable log concentration equations are:

$$\frac{dU_i^{s,stable}}{dz} = \frac{1 - \frac{1}{D_i(z)}}{1 - F(z)} \frac{dF}{dz} \quad (25)$$

$$\frac{dU_i^{f,stable}}{dz} = \frac{\frac{D_i^0}{D_i(z)} \exp(U_i^s(z) - U_i^f(z))}{F(z)} \frac{dF}{dz} \quad (26)$$

which are equivalent to a model for a fractionally melted residual solid and an accumulated fractional melt for the liquid.

Reincorporating this with the radiogenic component and scaling all distances by h gives the dimensionless equations:

$$\frac{dU_i^s}{d\zeta} = \frac{1 - \frac{1}{D_i(\zeta)}}{1 - F(\zeta)} \frac{dF}{d\zeta} + \frac{1 - \phi}{1 - F(\zeta)} \lambda'_i \left[\frac{\alpha_{i-1}^0}{\alpha_i^0} \exp[U_{i-1}^s(\zeta) - U_i^s(\zeta)] - 1 \right] \quad (27)$$

$$\frac{dU_i^f}{d\zeta} = \frac{\frac{D_i^0}{D_i(\zeta)} \exp(U_i^s(\zeta) - U_i^f(\zeta))}{F(\zeta)} + \frac{\rho_f \phi}{\rho_s F(\zeta)} \lambda'_i \left[\frac{D_{i-1}^0 \alpha_{i-1}^0}{D_i^0 \alpha_i^0} \exp[U_{i-1}^f(\zeta) - U_i^f(\zeta)] - 1 \right] \quad (28)$$

0.2.3 Solving for transport with chemical reactivity rates

The two models described above are end members for complete equilibrium and complete disequilibrium transport. For stable trace elements, these models produce melt compositions that are equivalent to batch melting and accumulated fractional melting (Spiegelman & Elliott (1993)). However, the actual transport of a reactive fluid (like a melt) through a solid matrix can fall anywhere between these end members depending on the rate of transport and re-equilibration between melt and solid, which can be sensitive to the mesoscopic geometry of melt and solid (Spiegelman & Kenyon (1992)). In an intermediate scenario, we envision that some reaction occurs, but chemical equilibration is incomplete due to slow reaction rates relative to the differential transport rates for the fluid and solid. If reaction times are sufficiently rapid to achieve chemical exchange over the lengthscale of interest before the liquid segregates, chemical equilibrium can be achieved; but for reactions that occur more slowly than effective transport rates, only partial chemical equilibrium can occur (Grose & Afonso (2019); Iwamori (1993, 1994); Kogiso et al. (2004); Liang & Liu (2016); Peate & Hawkesworth (2005); Qin et al. (1992); Yang et al. (2000)). Such reaction rates can include, for example, the rate of chemical migration over the distance between high porosity veins or channels (Aharonov et al. (1995); Jull et al. (2002); Spiegelman (2000); Stracke & Bourdon (2009); or, at the grain scale, the solid chemical diffusivity of elements over the diameter of individual mineral grains (Qin et al. (1992); Feineman & DePaolo (2003); Grose & Afonso (2019); Oliveira et al. (2020); Van Orman et al. (2002, 2006)).

To model this reactive transport scenario, we start with our equations for disequilibrium transport in a steady-state, one-dimensional conservative system, and add a chemical back-reaction term that permits exchange of elements between the fluid and the solid. The reaction term is scaled by a reactivity rate factor, \mathcal{R} and expressed in $\text{kg/m}^3/\text{yr}$. (i.e., the same units as the melting rate). The reactivity rate thus behaves much like the melting rate by governing the rate of exchange between the solid and liquid phases, effectively scaling the degree to which chemical exchange can occur. This new term could simulate a number of plausible scenarios that would physically limit the rate of chemical exchange

by transport along a given distance in a linear manner, such as the movement or diffusion of nuclides through the porous solid matrix between melt channels a given distance apart.

First, returning to the conservation of mass equations for a steady-state, one-dimensional, reactive system of stable trace elements, and using $\Gamma(z)$ to represent the melting rate:

$$\frac{d}{dz}\rho_f\phi w = \Gamma(z) \quad (29)$$

$$\frac{d}{dz}\rho_s(1-\phi)W = -\Gamma(z) \quad (30)$$

$$\frac{d}{dz}\rho_f\phi w c_i^f(z) = \frac{c_i^s(z)}{D_i(z)}\Gamma(z) - \Re\left(c_i^f(z) - \frac{c_i^s(z)}{D_i(z)}\right) \quad (31)$$

$$\frac{d}{dz}\rho_s(1-\phi)W c_i^s(z) = -\frac{c_i^s(z)}{D_i(z)}\Gamma(z) + \Re\left(c_i^f(z) - \frac{c_i^s(z)}{D_i(z)}\right) \quad (32)$$

where, for an adiabatic upwelling column,

$$\Gamma(z) = \rho_s W_0 \frac{dF}{dz} \quad (33)$$

From this, the equations (29) and (30) can be integrated (with appropriate boundary conditions at $z = 0$) to give

$$\rho_f\phi w = \rho_s W_0 F(z) \quad (34)$$

$$\rho_s(1-\phi)W = \rho_s W_0(1-F(z)) \quad (35)$$

Next, we expand the concentration equations to include the reactivity factor, and substitute the conservation of total mass determined above:

$$\rho_s W_0 F(z) \frac{d}{dz} c_i^f(z) + c_i^f(z) \Gamma(z) = \frac{c_i^s(z)}{D_i(z)} \Gamma(z) - \Re\left(c_i^f(z) - \frac{c_i^s(z)}{D_i(z)}\right) \quad (36)$$

$$\rho_s W_0(1-F(z)) \frac{d}{dz} c_i^s(z) - c_i^s(z) \Gamma(z) = -\frac{c_i^s(z)}{D_i(z)} \Gamma(z) + \Re\left(c_i^f(z) - \frac{c_i^s(z)}{D_i(z)}\right) \quad (37)$$

If we then combine the $\Gamma(z)$ terms and rearrange:

$$\rho_s W_0 F(z) \frac{d}{dz} c_i^f(z) = \Gamma(z) \left(\frac{c_i^s(z)}{D_i(z)} - c_i^f(z) \right) - \Re\left(c_i^f(z) - \frac{c_i^s(z)}{D_i(z)}\right) \quad (38)$$

$$\rho_s W_0(1-F(z)) \frac{d}{dz} c_i^s(z) = \Gamma(z) c_i^s(z) \left(1 - \frac{1}{D_i(z)} \right) + \Re\left(c_i^f(z) - \frac{c_i^s(z)}{D_i(z)}\right) \quad (39)$$

We can now divide the fluid and solid equations by c_i^f and c_i^s , respectively, and rearrange the W_0 terms:

$$\frac{1}{c_i^f(z)} \frac{dc_i^f}{dz} = \frac{1}{\rho_s W_0 F(z)} \left[\Gamma(z) \left(\frac{c_i^s(z)}{D_i(z) c_i^f(z)} - 1 \right) - \Re \left(1 - \frac{c_i^s(z)}{D_i(z) c_i^f(z)} \right) \right] \quad (40)$$

$$\frac{1}{c_i^s(z)} \frac{dc_i^s}{dz} = \frac{1}{\rho_s W_0 (1 - F(z))} \left[\Gamma(z) \left(1 - \frac{1}{D_i(z)} \right) + \frac{\Re}{D_i(z)} \left(\frac{D_i(z) c_i^f(z)}{c_i^s(z)} - 1 \right) \right] \quad (41)$$

220 The first terms on the right-hand side of each of these equations are identical to
 221 pure disequilibrium melting, such that if \Re is zero, the equations reduce to the disequi-
 222 librium transport case of Spiegelman & Elliott (1993).

223 To solve, the final terms that involve the reactivity factor can be further rewrit-
 224 ten using the definitions for U_i^f and U_i^s :

$$c_i^f(z) = c_{i,0}^f \exp[U_i^f(z)] = \frac{c_{i,0}^s}{D_i^0} \exp[U_i^f(z)] \quad (42)$$

$$c_i^s(z) = c_{i,0}^s \exp[U_i^s(z)] \quad (43)$$

225 Thus:

$$\frac{D_i(z) c_i^f(z)}{c_i^s(z)} = \frac{D_i(z)}{D_i^0} \exp[U_i^f(z) - U_i^s(z)] \quad (44)$$

$$\frac{c_i^s(z)}{D_i(z) c_i^f(z)} = \frac{D_i^0}{D_i(z)} \exp[U_i^s(z) - U_i^f(z)] \quad (45)$$

226 and:

$$\frac{dU_i^f}{dz} = \frac{1}{\rho_s W_0 F(z)} \left[\Gamma(z) \left(\frac{D_i^0}{D_i(z)} \exp[U_i^s(z) - U_i^f(z)] - 1 \right) - \Re \left(1 - \frac{D_i^0}{D_i(z)} \exp[U_i^s(z) - U_i^f(z)] \right) \right] \quad (46)$$

$$\frac{dU_i^s}{dz} = \frac{1}{\rho_s W_0 (1 - F(z))} \left[\Gamma(z) \left(1 - \frac{1}{D_i(z)} \right) + \frac{\Re}{D_i(z)} \left(\frac{D_i(z)}{D_i^0} \exp[U_i^f(z) - U_i^s(z)] - 1 \right) \right] \quad (47)$$

227 Finally, substituting adiabatic upwelling and scaling depth by h , and adding ra-
 228 dioactive terms gives the full solutions for the dimensionless equations $dU_i/d\zeta$:

$$\frac{dU_i^f}{d\zeta} = \frac{1}{F(\zeta)} \left[\frac{dF}{d\zeta} \left(\frac{D_i^0}{D_i(\zeta)} \exp[U_i^s(\zeta) - U_i^f(\zeta)] - 1 \right) \right] - \frac{\Re h}{\rho_s W_0 F(\zeta)} \left[1 - \frac{D_i^0}{D_i(\zeta)} \exp[U_i^s(\zeta) - U_i^f(\zeta)] \right] + \frac{\rho_f \phi}{\rho_s F} \lambda_i' \left[\frac{D_i^0 \alpha_{i-1}^0}{D_{i-1}^0 \alpha_i^0} \right] \quad (48)$$

$$\frac{dU_i^s}{d\zeta} = \frac{1}{(1 - F(\zeta))} \left[\frac{dF}{d\zeta} \left(1 - \frac{1}{D_i(\zeta)} \right) \right] + \frac{\Re h}{\rho_s W_0 D_i(\zeta) (1 - F(\zeta))} \left[\frac{D_i(\zeta)}{D_i^0} \exp[U_i^f(\zeta) - U_i^s(\zeta)] - 1 \right] + \frac{1 - \phi}{1 - F(\zeta)} \lambda_i' \left[\frac{\alpha_{i-1}^0}{\alpha_i^0} \right] \quad (49)$$

229 where h is the total height of the melting column.

0.2.3.1 The Damköhler number The dimensionless combination

$$Da = \frac{\Re h}{\rho_s W_0} \quad (50)$$

is the Damköhler number, which governs the reaction rate relative to the solid transport time. Damköhler numbers more generally are used to relate the timescales of chemical reactions to the rates of physical transport in a system. If re-equilibration is limited by solid state diffusion, \Re can be estimated using:

$$\Re \approx \frac{\rho_s \mathcal{D}_i}{d^2} \quad (51)$$

where \mathcal{D}_i is the *solid state* diffusivity of element i , and d is a nominal spacing between melt-channels (this spacing could, for example, be the average grain diameter for grain-scale channels, or 10 cm for closely spaced veins).

In this case (which we will assume for this paper), the Damköhler number can be written

$$Da = \frac{\mathcal{D}_i h}{W_0 d^2} \quad (52)$$

Substituting the definition of Da above yields the final dimensionless ODEs for the disequilibrium transport model:

$$\frac{dU_i^f}{d\zeta} = \frac{1}{F(\zeta)} \left(\frac{dF}{d\zeta} + Da \right) \left(\frac{D_i^0}{D_i(\zeta)} \exp[U_i^s(\zeta) - U_i^f(\zeta)] - 1 \right) + \frac{\rho_f \phi}{\rho_s F} \lambda'_i \left[\frac{D_i^0 \alpha_{i-1}^0}{D_{i-1}^0 \alpha_i^0} \exp[U_{i-1}^f(\zeta) - U_i^f(\zeta)] - 1 \right] \quad (53)$$

$$\frac{dU_i^s}{d\zeta} = \frac{1}{(1 - F(\zeta))} \left[\frac{dF}{d\zeta} \left(1 - \frac{1}{D_i(\zeta)} \right) + \frac{Da}{D_i(\zeta)} \left(\frac{D_i(\zeta)}{D_i^0} \exp[U_i^f(\zeta) - U_i^s(\zeta)] - 1 \right) \right] + \frac{1 - \phi}{1 - F(\zeta)} \lambda'_i \left[\frac{\alpha_{i-1}^0}{\alpha_i^0} \exp[U_{i-1}^s(\zeta) - U_i^s(\zeta)] - 1 \right] \quad (54)$$

with initial conditions $U_i^s = U_i^f = 0$.

In the limit where the Damköhler number approaches zero, the above formulas reduce to pure disequilibrium transport, whereas if Da approaches infinity (i.e., infinitely fast reactivity compared to physical transport), the system approaches equilibrium conditions ($c_i^s \rightarrow D_i c_i^f$).

0.2.3.2 Initial conditions Inspection of equation (53) shows that for the initial conditions described above and $F(0) = 0$, $\frac{dU_i^f}{d\zeta}$ is ill-defined (at least numerically in a floating-point system). However, taking the limit $\zeta \rightarrow 0$ and applying L'Hôpital's rule yields

$$\lim_{\zeta \rightarrow 0} \frac{dU_i^f}{d\zeta} = \frac{U_i'^s(0) - U_i'^f(0)}{F'(0)} \left(\frac{dF}{d\zeta} + Da \right) + \lambda'_i \left[\frac{D_i^0 \alpha_{i-1}^0}{D_{i-1}^0 \alpha_i^0} - 1 \right] \quad (55)$$

where

$$U_i'^s(0) = \left. \frac{dU_i^s}{d\zeta} \right|_{\zeta=0} \quad (56)$$

$$U_i'^f(0) = \left. \frac{dU_i^f}{d\zeta} \right|_{\zeta=0} \quad (57)$$

$$F'(0) = \left. \frac{dF}{d\zeta} \right|_{\zeta=0} \quad (58)$$

252 The initial radiogenic term also uses the limit from equation (34):

$$\lim_{\zeta \rightarrow 0} \frac{\rho_f \phi}{\rho_s F} = \frac{W_0}{w(0)} = 1 \quad (59)$$

253 Rearranging equation (55) gives the value for $U_i'^f(0)$ for $F = 0$ as

$$\lim_{\zeta \rightarrow 0} \frac{dU_i^f}{d\zeta} = \frac{1}{2 + \frac{Da}{F'(0)}} \left[U_i'^s(0) \left(1 + \frac{Da}{F'(0)} \right) + \lambda_i' \left[\frac{D_i^0 \alpha_{i-1}^0}{D_{i-1}^0 \alpha_i^0} - 1 \right] \right] \quad (60)$$

254 0.3 A pyUserCalc Jupyter notebook

255 0.3.1 Code design

256 The `UserCalc` Python package implements both equilibrium and reactive disequi-
 257 librium transport models and provides a set of code classes and utility functions for cal-
 258 culating and visualizing the results of one-dimensional, steady-state, partial melting for-
 259 ward models for both the ^{238}U and ^{235}U decay chains. The code package is organized
 260 into a set of Python classes and plotting routines, which are documented in the docstrings
 261 of the classes and also demonstrated in detail below. Here we briefly describe the over-
 262 all functionality and design of the code, which is open-source and can be modified to suit
 263 an individual researcher's needs. The code is currently available in a Git repository ([https://gitlab.com/ENKI-](https://gitlab.com/ENKI-portal/pyUsercalc)
 264 [portal/pyUsercalc](https://gitlab.com/ENKI-portal/pyUsercalc)), and any future edits or merge requests will be managed through Git-
 265 Lab.

266 The equilibrium and disequilibrium transport models described above have each
 267 been implemented as Python classes with a generic code interface:

```
268 '''
269 Interface:
270 - - - - -
271     model(alpha0, lambdas, D, W0, F, dFdZ, phi, rho_f=2800., rho_s=3300., method=method, Da=inf)
272
273 Parameters:
274 - - - - -
275     alpha0 : numpy array of initial activities
276     lambdas : numpy array of decay constants scaled by solid transport time
277     D : Function D(z) - - returns an array of partition coefficients at scaled height z
278     W0 : float - - Solid mantle upwelling rate
279     F : Function F(z) - - returns the degree of melting F
280     dFdZ : Function dFdZ(z) - - returns the derivative of F
281     phi : Function phi(z) - - returns the porosity
282     rho_f : float - - melt density
283     rho_s : float - - solid density
284     method : string - - ODE time -stepping scheme to be passed to solve_ivp (one of 'RK45', '1
285     Da : float - - Damköhler Number (defaults to \inf, unused in equilibrium model)
286
```

Required Method:

```

- - - - -
model.solve(): returns depth and log concentration numpy arrays z, Us, Uf
'''

```

which solves the scaled equations (i.e., equation (9) or equations (53) and (54)) for the log concentrations of nuclides U_i^s and U_i^f in a decay chain of arbitrary length, with scaled decay constants λ_i' and initial activity ratios α_i^0 . In the code, we use the variable z for the scaled height in the column (i.e. $z \equiv \zeta$), and the model equations assume a one-dimensional column with scaled height $0 \leq z \leq 1$. The bulk partition coefficients $D_i(z)$, degree of melting $F(z)$, melting rate $dF/dz(z)$, and porosity $\phi(z)$ are provided as functions of height in the column. Optional arguments include the melt and solid densities ρ_f and ρ_s , the Damköhler number Da , and the preferred numerical integration method (see `scipy.integrate.solve_ivp`). Some of these variables, such as $D_i(z)$ and $F(z)$, are provided by the user as described further below, and are then interpolated using model functions.

`UserCalc` provides two separate model classes, `EquilTransport` and `DisequilTransport`, for the different transport models; the user could add any other model that uses the same interface, if desired. Most users, however, will not access the models directly but rather through the driver class `UserCalc`, which provides support for solving and visualizing column models for the relevant ^{238}U and ^{235}U decay chains. The general interface for the `UserCalc` class is:

```

''' A class for constructing solutions for 1 -D, steady -state, open -system U -series transport
    as in Spiegelman (2000) and Elkins and Spiegelman (2021).

Usage:
- - - - -

us = UserCalc(df,dPdZ = 0.32373,n = 2.,tol=1.e -6,phi0 = 0.008,
              W0 =3.,model=EquilTransport,Da=None,stable=False,method='Radau')

Parameters:
- - - - -
df      : A pandas dataframe with columns ['P','F', Kr','DU','DTh','DRa','DPa']
dPdZ    : float - - Pressure gradient, to convert pressure P to depth z
n       : float - - Permeability exponent
tol     : float - - Tolerance for the ODE solver
phi0    : float - - Reference melt porosity
W0      : float - - Upwelling velocity (cm/yr)
model   : class - - A U -series transport model class (one of EquilTransport or Disequil
Da       : float - - Optional Da number for disequilibrium transport model
stable  : bool
          True: calculates concentrations for non -radiogenic nuclides with same chemical p
              (i.e. sets lambda=0)
          False: calculates the full radiogenic problem
method: string
          ODE time -stepping method to pass to solve_ivp
          (usually one of 'Radau', 'BDF', or 'RK45')
'''

```

The principal required data input is a spreadsheet containing the degree of melting $F(P)$, relative permeability $K_r(P)$, and bulk partition coefficients for the elements D_U , D_{Th} , D_{Ra} and D_{Pa} as functions of pressure P . The structure of the input data spread-

sheet is the same as that described in Spiegelman (2000), and is illustrated in Table 2 below. Because the user provides $F(z)$, $K_r(z)$, and bulk solid $D_i(z)$ input information to the model directly, any considerations such as mineral modes, mineral/melt D_i values, and productivity variations are external to this model and must be developed by the user separately. Once given this input spreadsheet by the user, the code routine initializes the decay constants for the isotopic decay chains and provides functions to interpolate $F(z)$ and $D_i(z)$ and calculate the porosity $\phi(z)$. Once thus initialized, the `UserCalc` class further provides the following methods:

```
'''
Principal Methods:
- - - - -
    phi                : returns porosity as a function of column height
    set_column_parameters : resets principal column parameters phi0, n, W0
    solve_1D            : 1D column solution for a single Decay chain
                        with arbitrary D, lambda, alpha_0
    solve_all_1D         : Solves a single column model for both 238U and 235U chains.
                        returns a pandas dataframe
    solve_grid           : Solves multiple column models for a grid of porosities and upwelling rates.
                        returns a 3 -D array of activity ratios
'''
```

Of these, the principal user-facing methods are:

- `UserCalc.solve_all_1D`, which returns a `pandas.DataFrame` table that contains, at each depth, solutions for the porosity (ϕ), the log concentrations of the specified nuclides in the ^{238}U and ^{235}U decay chains in both the melt and the solid, and the U-series activity ratios.
- `UserCalc.solve_grid`, which solves for a grid of one-dimensional solutions for different reference porosities (ϕ_0) and solid upwelling rates (W_0) and returns arrays of U-series activity ratios at a specified depth (usually the top of the column), as described in Spiegelman & Elliott (1993).

0.3.1.1 Visualization Functions In addition to the principal classes for calculating U-series activity ratios in partial melts, the `UserCalc` package also provides functions for visualizing model inputs and outputs. The primary plotting functions include:

- `UserCalc.plot_inputs(df)`: Visualizes the input dataframe to show $F(P)$, $K_r(P)$, and $D_i(P)$.
- `UserCalc.plot_1Dcolumn(df)`: Visualizes the output dataframe for a single one-dimensional melting column.
- `UserCalc.plot_contours(phi0, W0, act)`: Visualizes the output of `UserCalc.solve_grid` by generating contour plots of activity ratios at a specific depth as functions of the porosity (ϕ_0) and solid upwelling rate (W_0).
- `UserCalc.plot_mesh_Ra(Th, Ra, W0, phi0)` and `UserCalc.plot_mesh_Pa(Th, Pa, W0, phi0)`: Generates ‘mesh’ plots showing results for different ϕ_0 and W_0 values on $(^{226}\text{Ra}/^{230}\text{Th})$ vs. $(^{230}\text{Th}/^{238}\text{U})$ and $(^{231}\text{Pa}/^{235}\text{U})$ vs. $(^{230}\text{Th}/^{238}\text{U})$ activity diagrams.

Both the primary solver routines and visualization routines will be demonstrated in detail below.

0.3.1.2 Miscellaneous Convenience Functions Finally, the `UserCalc` module also provides a simple input spreadsheet generator similar to the one provided with the original `UserCalc` program of Spiegelman (2000). This tool is described more fully in the ac-

companion Jupyter notebook `twolayermodel.ipynb` in the Supplemental Materials, and has the interface:

```
• df = UserCalc.twolayermodel(P, F, Kr, D_lower, D_upper, N=100, P_lambda=1)
```

0.3.2 An example demonstrating *pyUserCalc* functionality for a single melting column

The Python code cells embedded below provide an example problem that demonstrates the use and behavior of the model for a simple, two-layer upwelling mantle column, with a constant melting rate within each layer and constant $K_r = 1$. This example is used to compare the outcomes from the original UserCalc equilibrium model Spiegelman (2000) to various other implementations of the code, such as pure disequilibrium transport and scaled reactivity rates, as described above.

To run the example code and use this article as a functioning Jupyter notebook, while in a web-enabled browser the user should select each embedded code cell below by mouse-click and then simultaneously type the ‘Shift’ and ‘Enter’ keys to run the cell, after which selection will automatically advance to the following cell. The first cell below imports necessary code libraries to access the Python toolboxes and functions that will be used in the rest of the program:

```
# Select this cell by mouse click, and run the code by simultaneously typing the 'Shift' + 'Enter'
# If the browser is able to run the Jupyter notebook, a number [1] will appear to the left of the cell

import pandas as pd
import numpy as np
import matplotlib.pyplot as plt
%matplotlib inline

# Import UserCalc:
import UserCalc
```

0.3.2.1 Entering initial input information and viewing input data In the full Jupyter notebook code available in the Git repository and provided here as Supplementary Materials, the user can edit a notebook copy and indicate their initial input data, as has been done for the sample data set below. The name for the user’s input data file should be set in quotes (i.e., replacing the word ‘sample’ in the cell below with the appropriate filename, minus the file extension). This name will be used both to find the input file and to label any output files produced. Our sample file can likewise be downloaded and used as a formatting template for other input files (see Supplementary Materials), and is presented as a useful example below. The desired input file should be saved to a ‘data’ folder in the notebook directory prior to running the code. If desired, a similarly simple two-layer input file can also be generated using the calculator tool provided in the supplementary code.

Once the cell has been edited to contain the correct input file name, the user should run the cell using the technique described above:

```
runname='sample'
```

The next cell below will read in the input data using the user filename specified above:

[H] [Input data table for example tested here, showing pressures in kbar (P), degree of melting (F), permeability coefficient (K_r), and bulk solid/melt partition coefficients

(D_i) for the elements of interest, U, Th, Ra, and Pa. This table illustrates the format required for input files for this model.

```

433 input_file = 'data/{}.csv'.format(runname)
434 df = pd.read_csv(input_file, skiprows=1, dtype=float)
435 df

```

	P	F	Kr	DU	DTh	DRa	DPa
436	0	40.0	0.00000	1.0	0.00900	0.00500	0.00002
437	1	39.0	0.00241	1.0	0.00900	0.00500	0.00002
438	2	38.0	0.00482	1.0	0.00900	0.00500	0.00002
439	3	37.0	0.00723	1.0	0.00900	0.00500	0.00002
440	4	36.0	0.00964	1.0	0.00900	0.00500	0.00002
441	5	35.0	0.01210	1.0	0.00900	0.00500	0.00002
442	6	34.0	0.01450	1.0	0.00900	0.00500	0.00002
443	7	33.0	0.01690	1.0	0.00900	0.00500	0.00002
444	8	32.0	0.01930	1.0	0.00900	0.00500	0.00002
445	9	31.0	0.02170	1.0	0.00900	0.00500	0.00002
446	10	30.0	0.02410	1.0	0.00900	0.00500	0.00002
447	11	29.0	0.02650	1.0	0.00900	0.00500	0.00002
448	12	28.0	0.02890	1.0	0.00900	0.00500	0.00002
449	13	27.0	0.03130	1.0	0.00900	0.00500	0.00002
450	14	26.0	0.03370	1.0	0.00900	0.00500	0.00002
451	15	25.0	0.03620	1.0	0.00900	0.00500	0.00002
452	16	24.0	0.03860	1.0	0.00900	0.00500	0.00002
453	17	23.0	0.04100	1.0	0.00899	0.00500	0.00002
454	18	22.0	0.04340	1.0	0.00893	0.00498	0.00002
455	19	21.0	0.04610	1.0	0.00852	0.00488	0.00002
456	20	20.0	0.05000	1.0	0.00700	0.00450	0.00002
457	21	19.0	0.05610	1.0	0.00548	0.00412	0.00002
458	22	18.0	0.06340	1.0	0.00507	0.00402	0.00002
459	23	17.0	0.07100	1.0	0.00501	0.00400	0.00002
460	24	16.0	0.07860	1.0	0.00500	0.00400	0.00002
461	25	15.0	0.08620	1.0	0.00500	0.00400	0.00002
462	26	14.0	0.09370	1.0	0.00500	0.00400	0.00002
463	27	13.0	0.10133	1.0	0.00500	0.00400	0.00002
464	28	12.0	0.10892	1.0	0.00500	0.00400	0.00002
465	29	11.0	0.11651	1.0	0.00500	0.00400	0.00002
466	30	10.0	0.12410	1.0	0.00500	0.00400	0.00002
467	31	9.0	0.13169	1.0	0.00500	0.00400	0.00002
468	32	8.0	0.13928	1.0	0.00500	0.00400	0.00002
469	33	7.0	0.14687	1.0	0.00500	0.00400	0.00002
470	34	6.0	0.15446	1.0	0.00500	0.00400	0.00002
471	35	5.0	0.16205	1.0	0.00500	0.00400	0.00002
472	36	4.0	0.16964	1.0	0.00500	0.00400	0.00002
473	37	3.0	0.17723	1.0	0.00500	0.00400	0.00002
474	38	2.0	0.18482	1.0	0.00500	0.00400	0.00002
475	39	1.0	0.19241	1.0	0.00500	0.00400	0.00002
476	40	0.0	0.20000	1.0	0.00500	0.00400	0.00002
477							

The next cell will visualize the input dataframe in Figure 0.3.2.1, using the utility function `plot_inputs`:

```

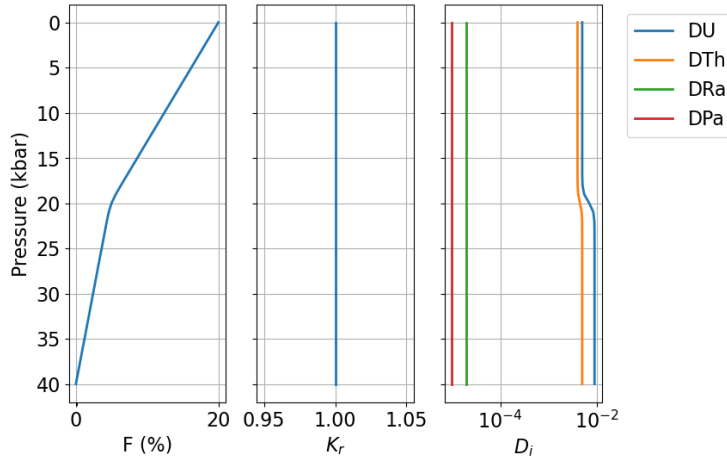
480                                     [H]

```

```

481 fig = UserCalc.plot_inputs(df)

```

Diagrams showing ex-

ample input parameters F , K_r , and D_i as a function of pressure, for the sample input file tested here.

0.3.2.2 Single column equilibrium transport model In its default mode, `UserCalc` solves the one-dimensional steady-state equilibrium transport model described in Spiegelman (2000). Below we will initialize the model, solve for a single column and plot the results.

First we set the physical parameters for the upwelling column and initial conditions:

```
# Maximum melt porosity:
phi0 = 0.008

# Solid upwelling rate in cm/yr. (to be converted to km/yr. in the driver function):
W0 = 3.

# Permeability exponent:
n = 2.

# Solid and liquid densities in kg/m3:
rho_s = 3300.
rho_f = 2800.

# Initial activity values (default is 1.0):
alpha0_238U = 1.
alpha0_235U = 1.
alpha0_230Th = 1.
alpha0_226Ra = 1.
alpha0_231Pa = 1.
alpha0_all = np.array([alpha0_238U, alpha0_230Th, alpha0_226Ra, alpha0_235U, alpha0_231Pa])
```

Next, we initialize the default equilibrium model:

```
us_eq = UserCalc.UserCalc(df)
```

and run the model for the input code and display the results for the final predicted melt composition in List 0.3.2.2:

[H]

```
df_out_eq = us_eq.solve_all_1D(phi0,n,W0,alpha0_all)
```

```
516 df_out_eq.tail(n=1)
```

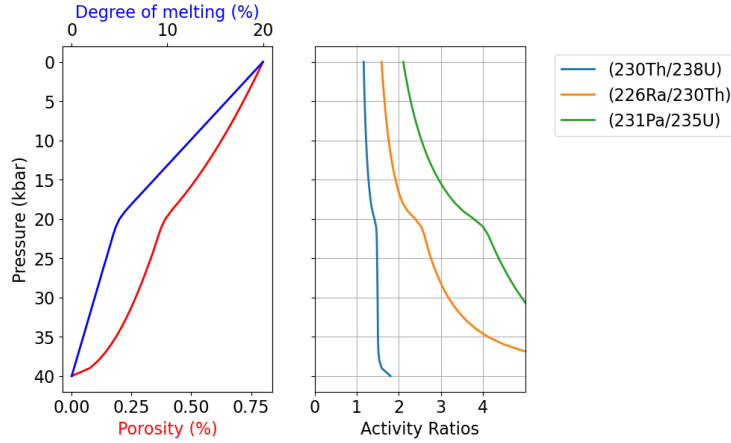
```
517 P depth F phi (230Th/238U) (226Ra/230Th) (231Pa/235U) \
518 40 0.0 0.0 0.2 0.008 1.164941 1.590091 2.10557
519
520 Uf_238U Uf_230Th Uf_226Ra Us_238U Us_230Th Us_226Ra Uf_235U \
521 40 -3.121055 -3.556171 -8.613841 -3.121055 -3.556171 -8.613841 -3.121909
522
523 Uf_231Pa Us_235U Us_231Pa
524 40 -9.179718 -3.121909 -9.179718
```

525 []Model output results for the equilibrium melting scenario tested above.

526 The cell below produces Figure 0.3.2.2, which shows the model results with depth:

527 [H]

```
528 fig = UserCalc.plot_1Dcolumn(df_out_eq)
```



529 []Equilibrium model out-
530 put results for the degree of melting, residual melt porosity, and activity ratios ($^{230}\text{Th}/^{238}\text{U}$),
531 ($^{226}\text{Ra}/^{230}\text{Th}$), and ($^{231}\text{Pa}/^{235}\text{U}$) as a function of pressure.

532 *0.3.2.3 Single column disequilibrium transport model* For comparison, we can
533 repeat the calculation using the disequilibrium transport model, and compare the results
534 to the equilibrium model. We first initialize a new model with $Da = 0$, which will cal-
535 culate full disequilibrium transport:

```
536 us_diseq = UserCalc.UserCalc(df, model=UserCalc.DisequilTransport, Da=0.)
```

537 The cells below calculate solutions for this pure disequilibrium scenario, as shown
538 in List 0.3.2.3:

539 [H]

```
540 df_out = us_diseq.solve_all_1D(phi0,n,W0,alpha0_all)
541 df_out.tail(n=1)
```

```
542 P depth F phi (230Th/238U) (226Ra/230Th) (231Pa/235U) \
543 40 0.0 0.0 0.2 0.008 1.051064 1.001056 1.055728
544
545 Uf_238U Uf_230Th Uf_226Ra Us_238U Us_230Th Us_226Ra Uf_235U \
546 40 -3.096781 -3.634765 -9.15517 -39.606679 -39.946072 -42.201858 -3.101977
```

```

547
548     Uf_231Pa    Us_235U    Us_231Pa
549 40 -9.850142 -39.636411 -45.498608

```

Model output results for the disequilibrium melting scenario tested above.

Next we compare the results to our equilibrium calculation above:

```

552
553 fig, axes = UserCalc.plot_1Dcolumn(df_out)
554 axes[2].set_prop_cycle(None)
555 for s in ['(230Th/238U)', '(226Ra/230Th)', '(231Pa/235U)']:
556     axes[2].plot(df_out_eq[s], df_out['P'], '-')
557     axes[2].plot(df_out_eq[s], df_out['P'], '.', color='grey')
558
559 axes[2].set_title('Da = {}'.format(us_diseq.Da))
560 plt.show()

```

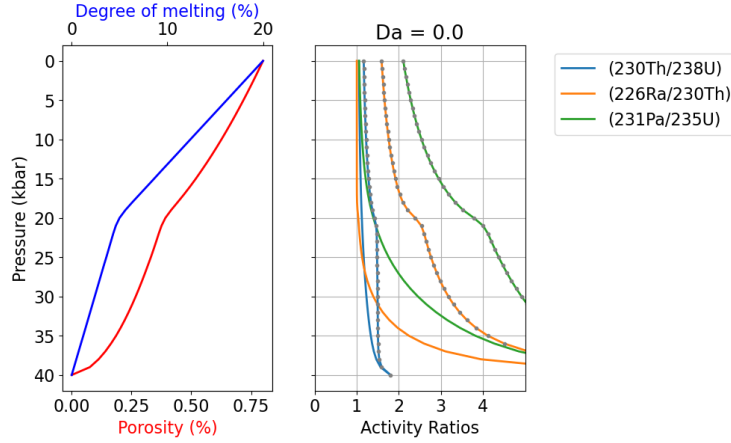


Figure 0.3.2.3 illustrates the disequilibrium model output results for the degree of melting, residual melt porosity, and activity ratios ($^{230}\text{Th}/^{238}\text{U}$), ($^{226}\text{Ra}/^{230}\text{Th}$), and ($^{231}\text{Pa}/^{235}\text{U}$) as a function of pressure, for the Damköhler number shown ($Da = 0$). For comparison, the curves with gray dots show solutions for the equilibrium transport model.

The dashed grey curves in Figure 0.3.2.3 illustrate the equilibrium transport solution, which is significantly different from the disequilibrium solution. If we increase the value of Da , however, the disequilibrium transport solution should converge towards the equilibrium scenario. To illustrate this, below we calculate the result for $Da = 1$:

```

570
571 # Reset the Da number in the reactive transport model to 1:
572 us_diseq.Da=1.
573
574 # Recalculate the model:
575 df_out = us_diseq.solve_all_1D(phi0,n,W0,alpha0_all)
576 df_out.tail(n=1)
577
578 P  depth    F    phi  (230Th/238U)  (226Ra/230Th)  (231Pa/235U)  \
579 40  0.0    0.0  0.2  0.008        1.158207        1.447593        1.917551
580
581     Uf_238U  Uf_230Th  Uf_226Ra  Us_238U  Us_230Th  Us_226Ra  Uf_235U  \

```

```

581 40 -3.112608 -3.553522 -8.70508 -3.959753 -4.02859 -7.428003 -3.117868
582
583 Uf_231Pa Us_235U Us_231Pa
584 40 -9.269214 -3.965023 -9.37465

```

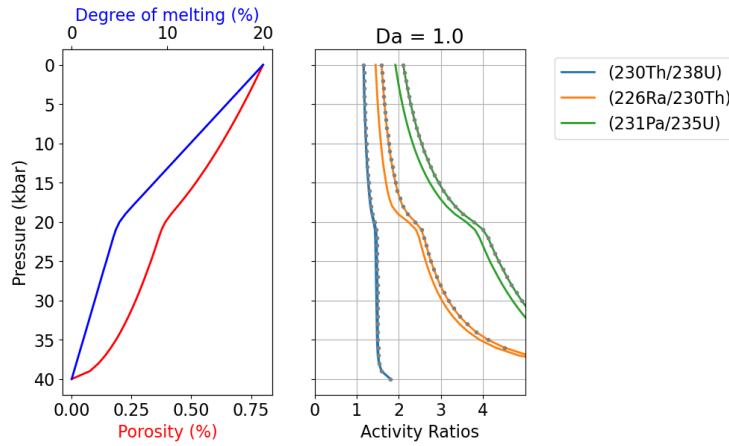
Model output results for the disequilibrium melting scenario tested above, where $Da = 1$.

[H]

```

588 fig, axes = UserCalc.plot_1Dcolumn(df_out)
589 axes[2].set_prop_cycle(None)
590 for s in ['(230Th/238U)', '(226Ra/230Th)', '(231Pa/235U)']:
591     axes[2].plot(df_out_eq[s], df_out['P'], '-')
592     axes[2].plot(df_out_eq[s], df_out['P'], '.', color='grey')
593 axes[2].set_title('Da = {}'.format(us_diseq.Da))
594 plt.show()

```



[Disequilibrium model output as in Figure 0.3.2.3, but for $Da = 1$.

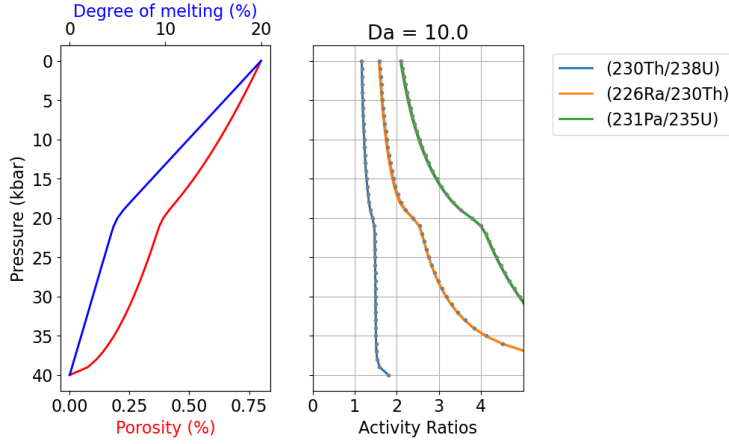
The outcome of the above calculation (Figure 0.3.2.3, List 0.3.2.3) approaches the equilibrium scenario more closely, as predicted. Below is an additional comparison for $Da = 10$:

[H]

```

601 # Reset the Da number in the reactive transport model to 10:
602 us_diseq.Da=10.
603
604 # Recalculate and plot the model:
605 df_out = us_diseq.solve_all_1D(phi0,n,W0,alpha0_all)
606
607 fig, axes = UserCalc.plot_1Dcolumn(df_out)
608 axes[2].set_prop_cycle(None)
609 for s in ['(230Th/238U)', '(226Ra/230Th)', '(231Pa/235U)']:
610     axes[2].plot(df_out_eq[s], df_out['P'], '-')
611     axes[2].plot(df_out_eq[s], df_out['P'], '.', color='grey')
612
613 axes[2].set_title('Da = {}'.format(us_diseq.Da))
614 plt.show()

```



[[Disequilibrium model

output as in Figure 0.3.2.3, but for $Da = 10$.

For $Da = 10$ (Figure 0.3.2.3), the activity ratios in the melt are indistinguishable from the equilibrium calculation, suggesting that a Damköhler number of 10 is sufficiently high for a melting system to approach chemical equilibrium, and illustrating that the equilibrium model of Spiegelman & Elliott (1993) and Spiegelman (2000) is the limiting case for the more general disequilibrium model presented here. For this problem, equilibrium transport always provides an upper bound on activity ratios.

0.3.2.4 Stable element concentrations For a stable element, i.e., $\lambda_i = 0$, Spiegelman & Elliott (1993) showed that the equilibrium melting model reduces identically to simple batch melting Shaw (1970), while the disequilibrium model with $Da = 0$ is equivalent to true fractional melting. This presents a useful test of the calculator that verifies the program is correctly calculating stable concentrations. To simulate stable element concentrations for U, Th, Ra, and Pa during equilibrium melting, we can use the same input file example as above and simply test the scenario where λ_i values are equal to zero.

First, we impose a “stable” condition that changes all decay constants $\lambda_i = 0$:

[H]

```
us_eq = UserCalc.UserCalc(df,stable=True)
df_out_eq = us_eq.solve_all_1D(phi0,n,W0,alpha0_all)
df_out_eq.tail(n=1)
```

```
P  depth    F    phi  (230Th/238U)  (226Ra/230Th)  (231Pa/235U)  \
40  0.0      0.0  0.2  0.008        1.003937        1.015919        1.019959

    Uf_238U  Uf_230Th  Uf_226Ra  Us_238U  Us_230Th  Us_226Ra  Uf_235U  \
40 -3.120895 -3.704753 -9.21042 -3.120895 -3.704753 -9.21042 -3.120895

    Uf_231Pa  Us_235U  Us_231Pa
40 -9.903528 -3.120895 -9.903528
```

[[Model output results for equilibrium porous flow melting where $\lambda_i = 0$, simulating stable element behavior for U, Th, Ra, and Pa and thus true (instantaneous) batch melting.

For comparison with the results in List 0.3.2.4, we can use the batch melting equation Shaw (1970) to calculate the concentrations of U, Th, Ra, and Pa using the input values in Table 2 for $F(z)$ and D_i , where:

$$\frac{c_i^f}{c_i^0} = \frac{1}{F + D_i(1 - F)} \quad (61)$$

and determine radionuclide activities for the batch melt using the definition of the activity a for a nuclide i :

$$a_i = \lambda_i c_i^f \quad (62)$$

and the initial nuclide activities a_i^0 , such that:

$$a_i = \frac{a_i^0}{F + D_i(1 - F)} \quad (63)$$

As the activity ratios in List 0.3.2.4 illustrate, the outcomes of this simple batch melting equation are identical to those produced by the model for equilibrium transport and $\lambda = 0$.

[H]

```
df_batch=df[['P','F','DU','DTh','DRa','DPa']]
df_batch['(230Th/238U)'] = (alpha0_all[1]/(df_batch.F -df_batch.F*df_batch.DTh+df_batch.DTh))/(
df_batch['(226Ra/230Th)'] = (alpha0_all[2]/(df_batch.F -df_batch.F*df_batch.DRa+df_batch.DRa))/(
df_batch['(231Pa/235U)'] = (alpha0_all[4]/(df_batch.F -df_batch.F*df_batch.DPa+df_batch.DPa))/(

# Extract columns and concatenate dataframes
cols = ['P', 'F', '(230Th/238U)', '(226Ra/230Th)', '(231Pa/235U)']
df_compare = pd.concat([ df_batch[cols].tail(1), df_out_eq[cols].tail(1)])
df_compare['model'] = ['Batch Melting', 'Equilibrium Transport: stable elements']
df_compare.set_index('model')

P      F  (230Th/238U)  (226Ra/230Th)  \
model
Batch Melting                0.0  0.2          1.003937          1.015919
Equilibrium Transport: stable elements  0.0  0.2          1.003937          1.015919

(231Pa/235U)
model
Batch Melting                1.019959
Equilibrium Transport: stable elements  1.019959
```

[Simple batch melting calculation results using the methods of Shaw (1970), demonstrating identical activity ratio results to those calculated using the equilibrium transport model with $\lambda_i = 0$.

Similarly, we can also determine pure disequilibrium melting using the disequilibrium transport model with $\lambda_i = 0$. A simple fractional melting problem is easiest to test using constant melt productivity and partitioning behavior, so here we test a simplified, one-layer scenario with constant dF/dz and D_i values:

[H]

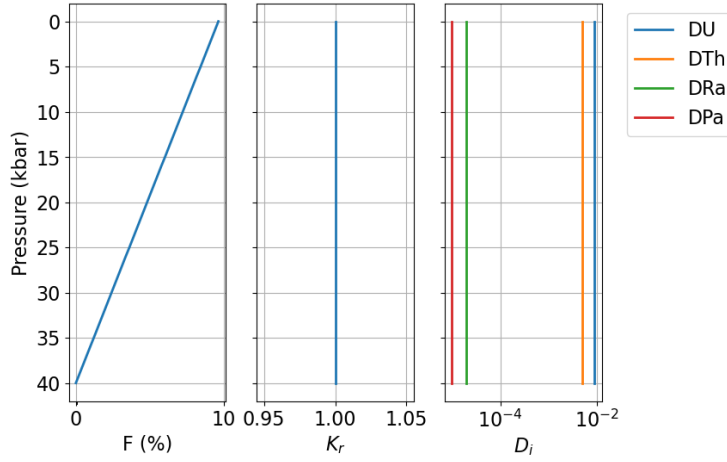
```
input_file_2 = 'data/simple_sample.csv'
df_test = pd.read_csv(input_file_2,skiprows=1,dtype=float)
UserCalc.plot_inputs(df_test)
```

```
df_test.tail(n=1)
```

```

P      F    Kr    DU    DTh    DRa    DPa
40  0.0  0.0964  1.0  0.009  0.005  0.00002  0.00001

```



Simple alternative input file with constant melt productivity and constant solid/melt partitioning, used here to test pure fractional melting outputs.

We note that numerical ordinary differential equation (ODE) solvers may not successfully solve for pure fractional melting with $Da = 0$ and stable elements, because the resulting extreme changes in solid concentrations for highly incompatible elements are difficult to resolve using numerical methods. Stable solutions can nonetheless be obtained for very small values of Da that approach $Da = 0$, and such solutions still provide a useful test of the disequilibrium transport model. Here we use $Da = 10^{-10}$; for such low Da values, the liquid closely approaches the composition of an accumulated fractional melt, and although the liquid and solid outcomes are slightly different from pure fractional melting, the solid is still essentially depleted of all incompatible nuclides.

```
us_diseq_test = UserCalc.UserCalc(df_test, model=UserCalc.DisequilTransport,stable=True,Da=1.e-10)
```

```
df_diseq_test = us_diseq_test.solve_all_1D(phi0,n,W0,alpha0_all)
```

Similar to our approach for equilibrium and batch melting, we can compare the results of disequilibrium transport for stable elements with pure fractional melting for constant partition coefficients using the definition of aggregated fractional melt concentrations (Figure 0.3.2.4):

$$\frac{c_i^s}{c_{i,0}^s} = (1 - F)^{1/D_i - 1} \quad (64)$$

$$\frac{c_i^f}{c_{i,0}^f} = \frac{D_i}{F} \left(1 - (1 - F)^{1/D_i} \right) \quad (65)$$

or in log units:

$$U_i^s = (1/D_i - 1) \log(1 - F) \quad (66)$$

$$U_i^f = \log \left(1 - (1 - F)^{1/D_i} \right) + \log \left(\frac{D_i}{F} \right) \quad (67)$$

```

709 df_frac=df_test[['P','F','DU','DTh','DRa','DPa']]
710 df_frac['(230Th/238U)'] = ((alpha0_all[1]/df_frac.F)*(1. -(1. -df_frac.F)**(1./df_frac.DTh))) /
711 df_frac['(226Ra/230Th)'] = ((alpha0_all[2]/df_frac.F)*(1. -(1. -df_frac.F)**(1./df_frac.DRa))) /
712 df_frac['(231Pa/235U)'] = ((alpha0_all[4]/df_frac.F)*(1. -(1. -df_frac.F)**(1./df_frac.DPa))) /

```

```

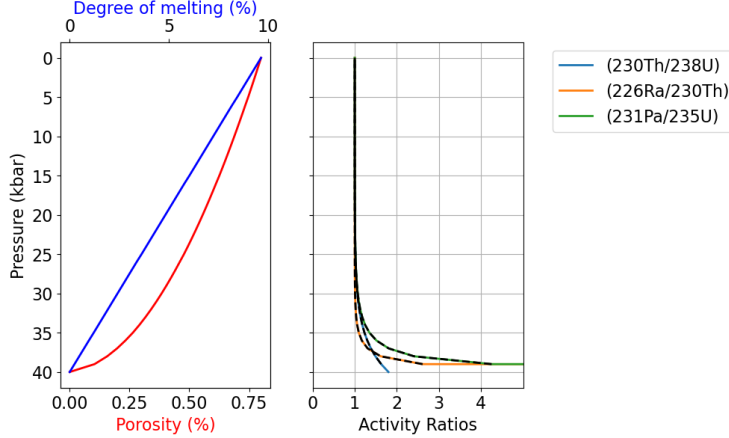
713 [H]

```

```

714 fig, axes = UserCalc.plot_1Dcolumn(df_diseq_test)
715 for s in ['(230Th/238U)', '(226Ra/230Th)', '(231Pa/235U)']:
716     axes[2].plot(df_frac[s], df_diseq_test['P'], '-', color='black')
717 plt.show()

```



718 [] Model output results
719 for the degree of melting, residual melt porosity, and activity ratios ($^{230}\text{Th}/^{238}\text{U}$), ($^{226}\text{Ra}/^{230}\text{Th}$),
720 and ($^{231}\text{Pa}/^{235}\text{U}$) as a function of pressure. The solid curves plot the results of pure frac-
721 tional melting for stable elements, while the dashed black curves illustrate the outcomes
722 of the disequilibrium transport model with $Da = 10^{-10}$ and $\lambda_i = 0$. The outcomes of
723 the two methods are indistinguishable.

724 *0.3.2.5 Considering lithospheric transport scenarios* In mantle decompression
725 melting scenarios, melting is expected to cease in the shallow, colder part of the regime
726 where a lithospheric layer is present. The effects of cessation of melting prior to reach-
727 ing the surface can be envisioned as affecting magma compositions in a number of ways,
728 some of which could be calculated using the models presented here by setting $dF = 0$.

729 There are, however, several limitations when using our transport models to simu-
730 late lithospheric melt transport in this way, as the model equations are written to track
731 steady-state decompression and melting. The first limitation is thus the underlying as-
732 sumption that the solid is migrating and experiences progressive melt depletion in the
733 model, while the solid lithosphere should in fact behave as a rigid matrix that does not
734 experience upwelling. For the disequilibrium transport model with $Da = 0$, no chem-
735 ical reequilibration occurs while $dF = 0$, so the lack of solid migration after the ces-
736 sation of melting does not pose a problem; instead, in the pure disequilibrium transport
737 case, imposing $dF = 0$ simply allows for radioactive decay and ingrowth during trans-
738 port through the lithospheric layer.

739 The equilibrium transport model, on the other hand, permits full equilibration even
740 if $dF = 0$, but the liquid composition does not directly depend on the solid concentra-
741 tion, $c_i^s(z)$, so ongoing chemical reequilibration between the liquid and a modified litho-
742 spheric solid could be simulated by modifying the bulk solid/liquid partition coefficients
743 D_i . However, the underlying model assumes that the liquid with mass proportion F_{max}
744 reequilibrates with the solid matrix in a steady-state transport regime, at the maximum
745 reference porosity, which may not accurately simulate the transport regime through the

fixed lithosphere with no melting. Because it does not directly consider mineral abundances or compositions, the model also does not account for complexities such as low temperature melt-rock reaction or mineral growth.

The case of the scaled disequilibrium transport model with $Da > 0$ is the most complex, since the model directly calculates reequilibration of the liquid with a progressively melting solid layer, and thus may not accurately simulate transport through the fixed solid lithosphere. We advise that if the model is used in this way, the results must be interpreted with additional caution.

Finally, calculating a given transport model through the upwelling asthenosphere and into a fixed overlying lithospheric layer neglects an additional, significant limitation: namely that melt-rock interactions, and thus the magma transport style, may be different in the lithosphere than in the melting asthenosphere. As noted above, this could also include low-temperature reactions and the growth of new mineral phases. While it is not possible to change transport models during a single 1D run in the current implementation, one alternative approach is to change the relative permeability, K_r , in the lithosphere, in addition to modifying the bulk partition coefficients to reflect lithospheric values. It may also be possible to run a separate, second-stage lithospheric calculation with modified input parameters and revised liquid porosity constraints, but this option is not currently implemented and would require an expansion of the current model.

Despite these caveats, there are some limited scenarios where users may wish to simulate equilibrium or disequilibrium magma transport through a capping layer with constant $dF = 0$, constant $\phi = \phi_0$, and revised D_i values for a modified layer mineralogy. The cells below provide options for modifying the existing input data table to impose such a layer. The first cell identifies a final melting pressure P_{Lithos} , which is defined by the user in kbar. This value can be set to 0.0 if no lithospheric cap is desired; in the example below, it has been set at 5.0 kbar. There are two overall options for how this final melting pressure could be used to modify the input data. One option (implemented in the Supplementary Materials but not tested here) simply deletes all lines in the input dataframe for depths shallower than P_{Lithos} . This is a straightforward option for a one-dimensional column scenario, where melting simply stops at the base of the lithosphere and the composition of the melt product is observed in that position. This is an effective way to limit further chemical interactions after melting has ceased; it fails to account for additional radioactive decay during lithospheric melt transport, but subsequent isotopic decay over a fixed transport time interval could then be calculated using the radioactive decay equations for U-series nuclides.

A second option, shown here to demonstrate outcomes, changes the degree of melting increments (dF) to a value of 0 for all depths shallower than P_{Lithos} , but allows model calculations to continue at shallower depths. This is preferable if the user aims to track additional radioactive decay and/or chemical exchange after melting has ceased and during subsequent transport through the lithospheric layer, and shall be explored further below.

```
Plithos = 5.0
```

```
Pfinal = df.iloc[(df['P'] - Plithos).abs().idxmin()]
F_max = Pfinal[1].tolist()
df.loc[(df['P'] < Plithos), ['F']] = F_max
```

For equilibrium transport scenarios, the cell below offers one possible option for modifying lithospheric solid/melt bulk partition coefficients. We note that if the disequilibrium transport model is used with $Da = 0$ (i.e., pure chemical disequilibrium), this cell is not necessary.

The option demonstrated below imposes new, constant melt-rock partition coefficients during lithospheric transport. These values are assumed to be fixed. An alternative choice, included in the Supplementary Materials, instead fixes the shallower lithospheric solid/melt bulk partition coefficients such that they are equal to D_i values at the depth where melting ceased (i.e., P_{Lithos}).

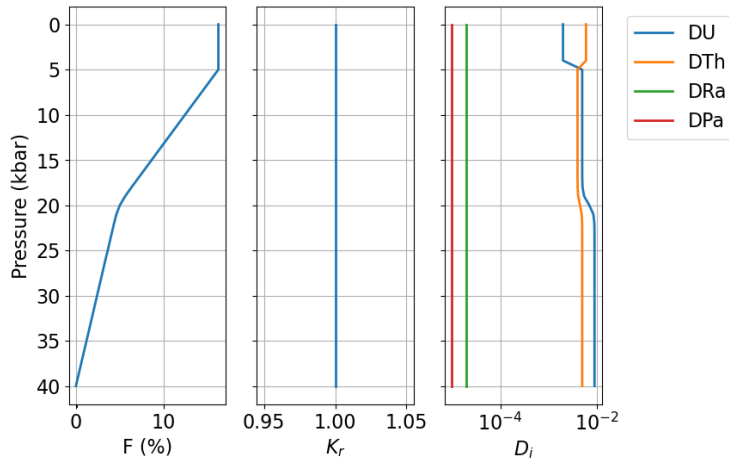
```
# Define new bulk solid/liquid partition coefficients for the lithospheric layer:
D_U_lith = 0.002
D_Th_lith = 0.006
D_Ra_lith = 0.00002
D_Pa_lith = 0.00001

# Implement the changed values defined above:
df.loc[(df['P'] < Plithos),['DU']] = D_U_lith
df.loc[(df['P'] < Plithos),['DTh']] = D_Th_lith
df.loc[(df['P'] < Plithos),['DRa']] = D_Ra_lith
df.loc[(df['P'] < Plithos),['DPa']] = D_Pa_lith
```

Following any changes implemented above, the cells below will process and display the refined input data (Figure 0.3.2.5, Table 0.3.2.5).

[H]

```
fig=UserCalc.plot_inputs(df)
```



Diagrams showing in-

put parameters F , K_r , and D_i as a function of pressure, for the example input file and modified lithospheric conditions.

[H] Input data table for an example scenario with modified lithospheric transport conditions, showing pressures in kbar (P), degree of melting (F), permeability coefficient (K_r), and bulk solid/melt partition coefficients (D_i) for the elements of interest, U, Th, Ra, and Pa.

df

P	F	Kr	DU	DTh	DRa	DPa	
0	40.0	0.00000	1.0	0.00900	0.00500	0.00002	0.00001
1	39.0	0.00241	1.0	0.00900	0.00500	0.00002	0.00001
2	38.0	0.00482	1.0	0.00900	0.00500	0.00002	0.00001
3	37.0	0.00723	1.0	0.00900	0.00500	0.00002	0.00001
4	36.0	0.00964	1.0	0.00900	0.00500	0.00002	0.00001

```

830 5 35.0 0.01210 1.0 0.00900 0.00500 0.00002 0.00001
831 6 34.0 0.01450 1.0 0.00900 0.00500 0.00002 0.00001
832 7 33.0 0.01690 1.0 0.00900 0.00500 0.00002 0.00001
833 8 32.0 0.01930 1.0 0.00900 0.00500 0.00002 0.00001
834 9 31.0 0.02170 1.0 0.00900 0.00500 0.00002 0.00001
835 10 30.0 0.02410 1.0 0.00900 0.00500 0.00002 0.00001
836 11 29.0 0.02650 1.0 0.00900 0.00500 0.00002 0.00001
837 12 28.0 0.02890 1.0 0.00900 0.00500 0.00002 0.00001
838 13 27.0 0.03130 1.0 0.00900 0.00500 0.00002 0.00001
839 14 26.0 0.03370 1.0 0.00900 0.00500 0.00002 0.00001
840 15 25.0 0.03620 1.0 0.00900 0.00500 0.00002 0.00001
841 16 24.0 0.03860 1.0 0.00900 0.00500 0.00002 0.00001
842 17 23.0 0.04100 1.0 0.00899 0.00500 0.00002 0.00001
843 18 22.0 0.04340 1.0 0.00893 0.00498 0.00002 0.00001
844 19 21.0 0.04610 1.0 0.00852 0.00488 0.00002 0.00001
845 20 20.0 0.05000 1.0 0.00700 0.00450 0.00002 0.00001
846 21 19.0 0.05610 1.0 0.00548 0.00412 0.00002 0.00001
847 22 18.0 0.06340 1.0 0.00507 0.00402 0.00002 0.00001
848 23 17.0 0.07100 1.0 0.00501 0.00400 0.00002 0.00001
849 24 16.0 0.07860 1.0 0.00500 0.00400 0.00002 0.00001
850 25 15.0 0.08620 1.0 0.00500 0.00400 0.00002 0.00001
851 26 14.0 0.09370 1.0 0.00500 0.00400 0.00002 0.00001
852 27 13.0 0.10133 1.0 0.00500 0.00400 0.00002 0.00001
853 28 12.0 0.10892 1.0 0.00500 0.00400 0.00002 0.00001
854 29 11.0 0.11651 1.0 0.00500 0.00400 0.00002 0.00001
855 30 10.0 0.12410 1.0 0.00500 0.00400 0.00002 0.00001
856 31 9.0 0.13169 1.0 0.00500 0.00400 0.00002 0.00001
857 32 8.0 0.13928 1.0 0.00500 0.00400 0.00002 0.00001
858 33 7.0 0.14687 1.0 0.00500 0.00400 0.00002 0.00001
859 34 6.0 0.15446 1.0 0.00500 0.00400 0.00002 0.00001
860 35 5.0 0.16205 1.0 0.00500 0.00400 0.00002 0.00001
861 36 4.0 0.16205 1.0 0.00200 0.00600 0.00002 0.00001
862 37 3.0 0.16205 1.0 0.00200 0.00600 0.00002 0.00001
863 38 2.0 0.16205 1.0 0.00200 0.00600 0.00002 0.00001
864 39 1.0 0.16205 1.0 0.00200 0.00600 0.00002 0.00001
865 40 0.0 0.16205 1.0 0.00200 0.00600 0.00002 0.00001

```

866 The cells below will rerun the end member models for the modified lithospheric in-
867 put file. First, for equilibrium transport:

```

868 us_eq = UserCalc.UserCalc(df,stable=False)
869 df_out_eq = us_eq.solve_all_1D(phi0,n,W0,alpha0_all)

```

870 And second, for disequilibrium transport with $Da = 0$:

```

871 us_diseq = UserCalc.UserCalc(df,model=UserCalc.DisequilTransport,Da=0,stable=False)
872 df_out_diseq = us_diseq.solve_all_1D(phi0,n,W0,alpha0_all)

```

873 List 0.3.2.5 below displays the activity ratios determined for the final melt com-
874 positions at the end of the two simulations (i.e., the tops of the one-dimensional melt-
875 ing columns).

876 [H]

```

877 df_compare = pd.concat([df_out_eq.tail(n=1), df_out_diseq.tail(n=1)])

```

```

878 df_compare['model'] = ['Equilibrium Transport', 'Disequilibrium Transport']
879 df_compare.set_index('model')

880 P depth      F    phi  (230Th/238U)  \
881 model
882 Equilibrium Transport    0.0    0.0  0.16205  0.008    1.015792
883 Disequilibrium Transport    0.0    0.0  0.16205  0.008    1.039707
884
885          (226Ra/230Th)  (231Pa/235U)  Uf_238U  Uf_230Th  \
886 model
887 Equilibrium Transport    1.894057    1.792975 -2.901132 -3.473250
888 Disequilibrium Transport    1.000828    1.034615 -2.890415 -3.439263
889
890          Uf_226Ra    Us_238U    Us_230Th    Us_226Ra    Uf_235U  \
891 model
892 Equilibrium Transport -8.355990 -2.901132 -3.473250 -8.355990 -2.902001
893 Disequilibrium Transport -8.959896 -30.344939 -30.346082 -30.346108 -2.891481
894
895          Uf_231Pa    Us_235U    Us_231Pa
896 model
897 Equilibrium Transport -9.120520 -2.902001 -9.120520
898 Disequilibrium Transport -9.659847 -30.359772 -30.359742

```

Model output results for the disequilibrium ($Da = 0$) melting scenarios tested here, with modified lithospheric input conditions.

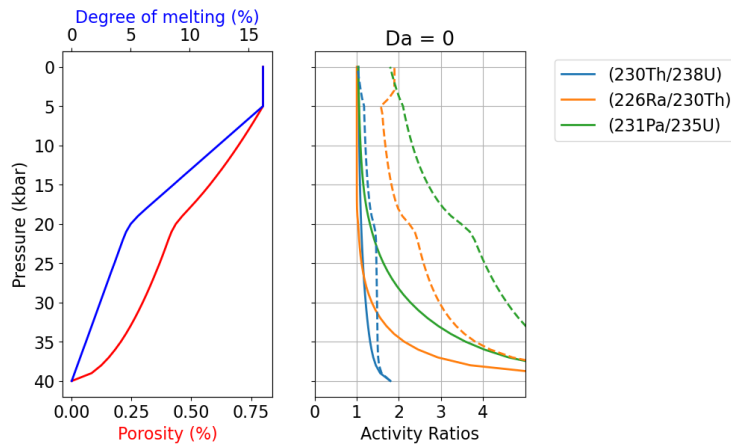
The following cell generates Figure 0.3.2.5, which illustrates outcomes with depth for the equilibrium and disequilibrium transport models. The model outcomes for the two transport scenarios are notably different, particularly for the shorter-lived isotopic pairs.

[H]

```

906 fig, axes = UserCalc.plot_1Dcolumn(df_out_diseq)
907 axes[2].set_prop_cycle(None)
908 for s in ['(230Th/238U)', '(226Ra/230Th)', '(231Pa/235U)']:
909     axes[2].plot(df_out_eq[s], df_out['P'], '- -')
910 axes[2].set_title('Da = {}'.format(us_diseq.Da))
911 plt.show()

```



Comparison of equilibrium (dashed) and disequilibrium ($Da = 0$; solid) transport model output results for the degree of melting, residual melt porosity, and activity ratios ($^{230}\text{Th}/^{238}\text{U}$), ($^{226}\text{Ra}/^{230}\text{Th}$),

and ($^{231}\text{Pa}/^{235}\text{U}$) as a function of pressure, for the modified lithospheric transport scenario explored above. Symbols and lines as in Figure 0.3.2.3.

0.3.3 Batch operations

For many applications, it is preferable to calculate an ensemble of model scenarios over a range of input parameters directly related to questions about the physical constraints on melt generation, such as the maximum residual or reference melt porosity (ϕ_0) and the solid mantle upwelling rate (W_0). The cells below determine a series of one-dimensional column results for the equilibrium transport model and the parameters defined above (that is, the input conditions shown in Table 0.3.2.5 with $n = 2$, $\rho_s = 3300 \text{ kg/m}^3$, and $\rho_f = 2800 \text{ kg/m}^3$), but over a range of values for ϕ_0 and W_0 ; these results are then shown in a series of figures. The user can select whether to define the specific ϕ_0 and W_0 values as evenly spaced log grid intervals (Option 1) or with manually specified values (Option 2). As above, all upwelling rates are entered in units of cm/yr. We note that because some of these models tend to be stiff and the Radau ODE solver is relatively computationally expensive, the batch operations below may require a few minutes of computation time for certain scenarios. Here we show the results for the default equilibrium model over a range of selected ϕ_0 and W_0 values of interest:

```
# Option 1 (evenly spaced log grid intervals):
# phi0 = np.logspace( -3, -2,11)
# W0 = np.logspace( -1,1,11)

# Option 2 (manual selection of values):
phi0 = np.array([0.001, 0.002, 0.005, 0.01])
W0 = np.array([0.5, 1., 2., 5., 10., 20., 50.])

import time
tic = time.perf_counter()
toc = time.perf_counter()

# Calculate the U -238 decay chain grid values:
act = us_eq.solve_grid(phi0, n, W0, us_eq.D_238, us_eq.lambdas_238, us_eq.alphas_238)
Th = act[0]
Ra = act[1]
df = pd.DataFrame(Th)
df = pd.DataFrame(Ra)

W = 0.5 . . . .
W = 1.0 . . . .
W = 2.0 . . . .
W = 5.0 . . . .
W = 10.0 . . . .
W = 20.0 . . . .
W = 50.0 . . . .

# Calculate the U -235 decay chain grid values:
act_235 = us_eq.solve_grid(phi0, n, W0, us_eq.D_235, us_eq.lambdas_235, us_eq.alphas_235)
Pa = act_235[0]
df = pd.DataFrame(Pa)

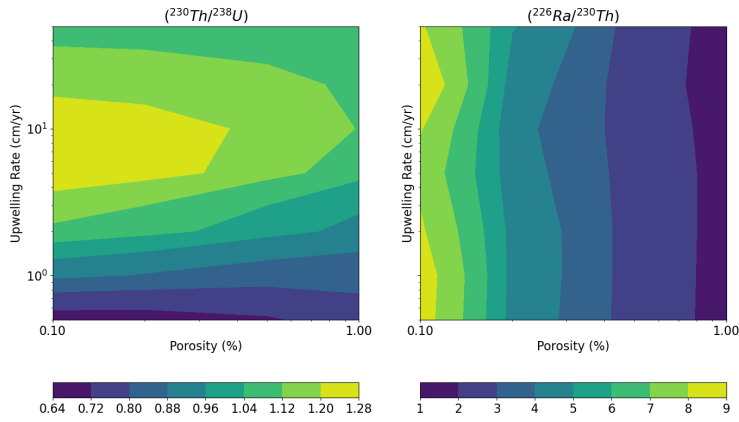
W = 0.5 . . . .
W = 1.0 . . . .
W = 2.0 . . . .
```

962 $W = 5.0$
 963 $W = 10.0$
 964 $W = 20.0$
 965 $W = 50.0$

966 The figures below illustrate the batch model results in a variety of ways. First, each
 967 isotopic activity ratio is contoured in ϕ_0 vs. W_0 space (Figure 0.3.3), using figures sim-
 968 ilar to the contour plots of Spiegelman (2000). The model outcomes for W_0 and ϕ_0 val-
 969 ues are also contoured as mesh “grids” in activity ratio-activity ratio plots (Figure 0.3.3).
 970 These diagrams show the outcomes for model runs with a given W_0 and ϕ_0 value at each
 971 grid intersection point, and each curve shows outcomes for a constant W_0 value with vari-
 972 able ϕ_0 or vice versa, as indicated in the figure legend. Because this particular example
 973 shows results for the equilibrium transport model, and the input values for the shallow,
 974 spinel peridotite layer of the sample input file define $D_U < D_{Th}$, we note that some of
 975 the results exhibit $(^{230}\text{Th}/^{238}\text{U}) < 1.0$ in Figure 0.3.3.

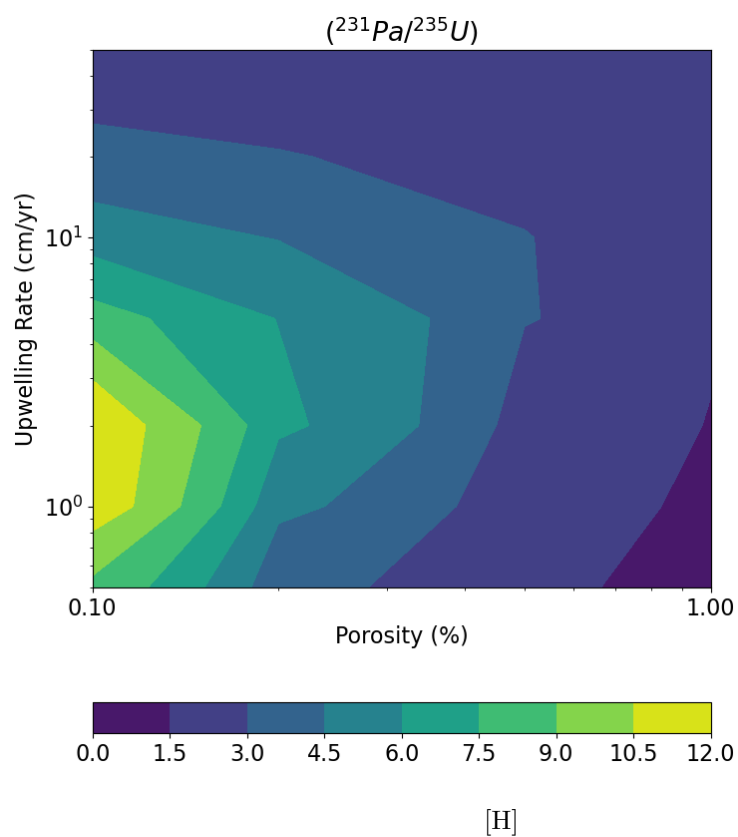
976 [H]

977 `UserCalc.plot_contours(phi0,W0,act, figsize=(8,10))`



978 [Diagrams of upwelling
 979 rate (W_0) vs. maximum residual melt porosity (ϕ) showing contoured activity ratios for
 980 $(^{230}\text{Th}/^{238}\text{U})$ (top panel), $(^{226}\text{Ra}/^{230}\text{Th})$ (middle panel), and $(^{231}\text{Pa}/^{235}\text{U})$ (bottom panel).
 981

982 `UserCalc.plot_contours(phi0,W0,act_235,figsize=(8,10))`

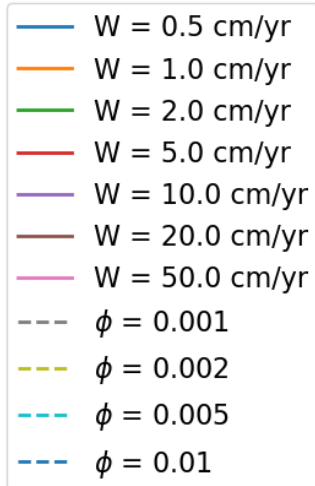
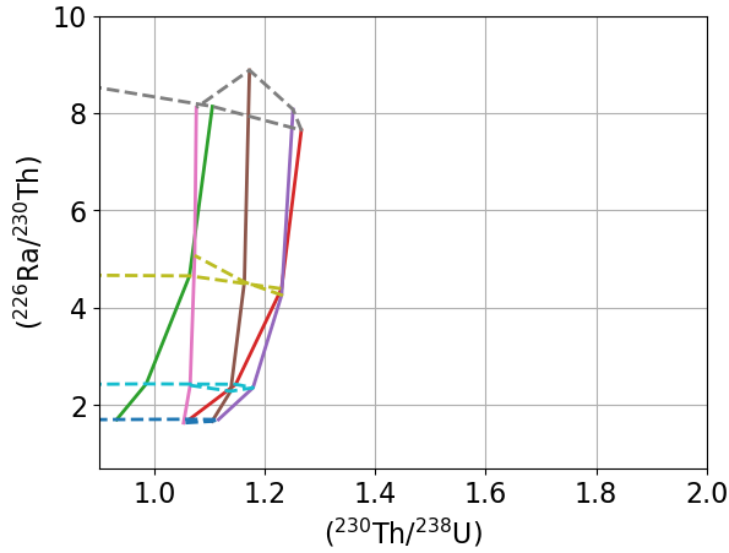


983

984

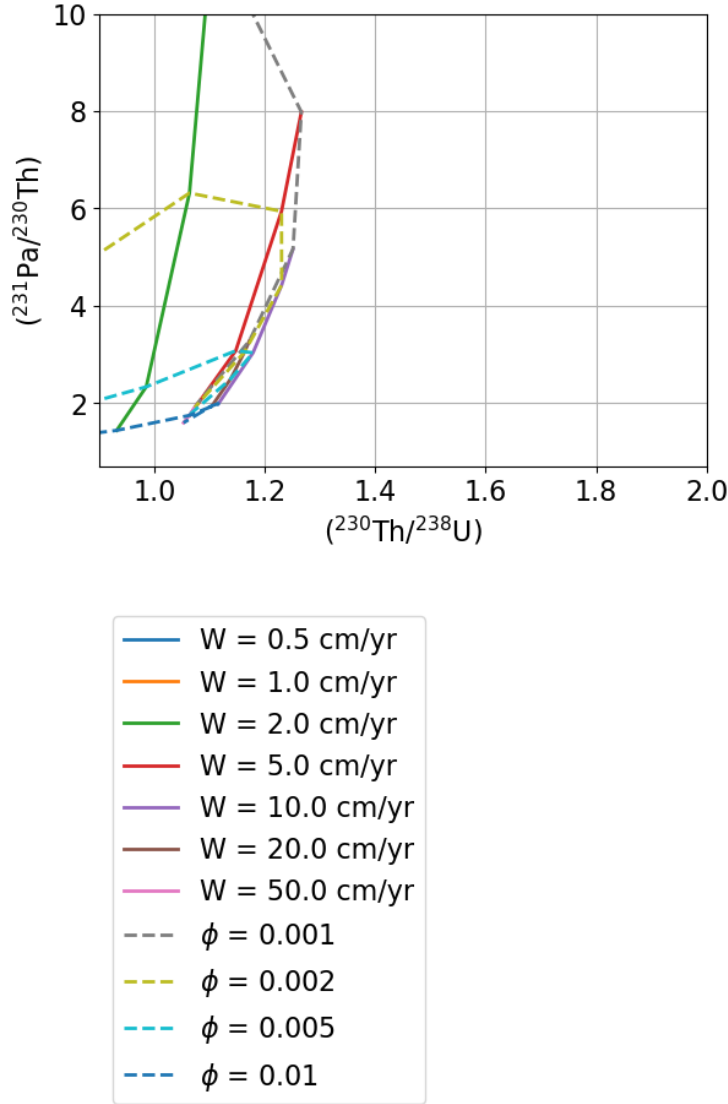
985

UserCalc.plot_mesh_Ra(Th,Ra,W0,phi0)



Diagrams showing $(^{226}\text{Ra}/^{230}\text{Th})$ vs. $(^{230}\text{Th}/^{238}\text{U})$ (top) and $(^{231}\text{Pa}/^{235}\text{U})$ vs. $(^{230}\text{Th}/^{238}\text{U})$ (bottom) for the gridded upwelling rate (W_0) and maximum residual porosity (ϕ) values defined above.

UserCalc.plot_mesh_Pa(Th,Pa,W0,phi0)



990

991 0.4 Summary

992 We present pyUserCalc, an expanded, publicly available, open-source version of the
 993 UserCalc code for determining U-series disequilibria generated in basalts by one-dimensional,
 994 decompression partial melting. The model has been developed from conservation of mass
 995 equations with two-phase (solid and liquid) porous flow and permeability governed by
 996 Darcy's Law. The model reproduces the functionality of the original UserCalc equilib-
 997 rium porous flow calculator Spiegelman (2000) in pure Python code, and implements a
 998 new disequilibrium transport model. The disequilibrium transport code includes reac-
 999 tivity rate-limited chemical equilibration calculations controlled by a Damköhler num-
 1000 ber, Da . For stable elements with decay constants equal to zero, the equilibrium model
 1001 reduces to batch melting and the disequilibrium transport model with $Da = 0$ to pure
 1002 fractional melting. The method presented here can be extended to other applications in
 1003 geochemical porous flow calculations in future work.

1004 Open Research

1005 The data set for this research consists of a code package, which is available in sev-
 1006 eral ways: 1) in the supporting information, 2) through a binder container (at <https://mybinder.org/v2/gl/ENKI->

portal%2FpyUsercalc/master?filepath=pyUserCalc_manuscript.ipynb), and 3) in the ENKI
 GitLab data repository (<https://gitlab.com/ENKI-portal/pyUsercalc>), which can also
 be accessed at the ENKI cloud server (<https://server.enki-portal.org/hub/login>) with
 a free GitLab account (register at <https://gitlab.com/ENKI-portal>). The primary source
 for pyUserCalc is also hosted in the ENKI GitLab repository, and any future issues and
 merge requests will be handled there.

Acknowledgments

We thank three anonymous reviewers for thoughtful feedback that strengthened this manuscript.
 We also thank K.W.W. Sims and P. Kelemen for initiating early discussions about cre-
 ating a new porous flow disequilibrium transport calculator back in 2008, and M. Ghiorso
 for inviting L. Elkins to join the ENKI working group and thereby catalyzing this fresh
 effort. We further thank the ENKI working group for their helpful suggestions and feed-
 back. L. Elkins received ENKI working group travel assistance that contributed to this
 research effort, and was supported by NSF award OCE-1658011. M. Spiegelman was sup-
 ported by the ENKI NSF SI² award NSF-ACI1550337. This work is dedicated to the mem-
 ory of our colleague, mentor, and friend Peter Fox, who encouraged our work on this project,
 expertly handled this manuscript, and spearheaded exciting innovations like publishing
 executable code in *Earth and Space Science*.

References

- Aharonov, E., Whitehead, J. A., Kelemen, P., & Spiegelman, M. (1995). Channeling
 instability of upwelling melt in the mantle. *Journal of Geophysical Research: Solid
 Earth*, 100(B10), 20433–20450. doi: 10.1029/95jb01307
- Bourdon, B., Turner, S. P., & Ribe, N. M. (2005). Partial melting and upwelling
 rates beneath the azores from a u-series isotope perspective. *Earth and Planetary
 Science Letters*, 239, 42–56. doi: 10.1016/j.epsl.2005.08.008
- Elkins, L. J., Bourdon, B., & Lambart, S. (2019). Testing pyroxenite versus peri-
 dotite sources for marine basalts using u-series isotopes. *Lithos*, 332–333, 226–244.
 doi: 10.1016/j.lithos.2019.02.011
- Elkins, L. J., & Spiegelman, M. (2021, December). pyusercalc: A revised jupyter
 notebook calculator for uranium-series disequilibria in basalts. *Earth and Space
 Science*, 8(12). Retrieved from <http://dx.doi.org/10.1029/2020EA001619> doi:
 10.1029/2020ea001619
- Feineman, M. D., & DePaolo, D. J. (2003). Steady-state ²²⁶Ra/²³⁰Th disequilibrium
 in mantle minerals: Implications for melt transport rates in island arcs. *Earth and
 Planetary Science Letters*, 215(3–4), 339–355. doi: 10.1016/s0012-821x(03)00454-
 0
- Grose, C. J., & Afonso, J. C. (2019). Chemical disequilibria, lithospheric thickness,
 and the source of ocean island basalts. *Journal of Petrology*, 60(4), 755–790. doi:
 10.1093/petrology/egz012
- Iwamori, H. (1993). Dynamic disequilibrium melting model with porous flow and
 diffusion-controlled chemical equilibration. *Earth and Planetary Science Letters*,
 114(2–3), 301–313. doi: 10.1016/0012-821x(93)90032-5
- Iwamori, H. (1994). ²³⁸u-²³⁰th-²²⁶ra and ²³⁵u-²³¹pa disequilibria produced by mantle
 melting with porous and channel flows. *Earth and Planetary Science Letters*, 125,
 1–16. doi: 10.1016/0012-821x(94)90203-8
- Jull, M., Kelemen, P., & Sims, K. (2002). Consequences of diffuse and channelled
 porous melt migration on uranium series disequilibria. *Geochimica et Cosmochim-
 ica Acta*, 66, 4133–4148. doi: 10.1016/s0016-7037(02)00984-5
- Kogiso, T., Hirschmann, M. M., & Reiners, P. W. (2004). Length scales of
 mantle heterogeneities and their relationship to ocean island basalt geochem-
 istry. *Geochimica et Cosmochimica Acta*, 68(2), 345–360. doi: 10.1016/

- s0016-7037(03)00419-8
- Liang, Y., & Liu, B. (2016). Simple models for disequilibrium fractional melting and batch melting with application to ree fractionation in abyssal peridotites. *Geochimica et Cosmochimica Acta*, 173, 181–197. doi: 10.1016/j.gca.2015.10.020
- Lundstrom, C., Gill, J., & Williams, Q. (2000). A geochemically consistent hypothesis for morb generation. *Chemical Geology*, 162(2), 105–126. doi: 10.1016/s0009-2541(99)00122-9
- McKenzie, D. (1985). Th-230-u-238 disequilibrium and the melting processes beneath ridge axes. *Earth and Planetary Science Letters*, 72(2–3), 149–157. doi: 10.1016/0012-821x(85)90001-9
- Miller, K. J., Zhu, W. L., Montési, L. G., & Gaetani, G. A. (2014). Experimental quantification of permeability of partially molten mantle rock. *Earth and Planetary Science Letters*, 388, 273–282.
- Oliveira, B., Afonso, J. C., & Tilhac, R. (2020). A disequilibrium reactive transport model for mantle magmatism. *Journal of Petrology*. doi: 10.1093/petrology/egaa067
- Peate, D. W., & Hawkesworth, C. J. (2005). U series disequilibria: Insights into mantle melting and the timescales of magma differentiation. *Reviews of Geophysics*, 43(1). doi: 10.1029/2004rg000154
- Qin, Z., Lu, F., & Anderson, A. T. (1992). Diffusive reequilibration of melt and fluid inclusions. *American Mineralogist*, 77(5–6), 565–576.
- Shaw, D. M. (1970). Trace element fractionation during anatexis. *Geochimica et Cosmochimica Acta*, 34(2), 237–243. doi: 10.1016/0016-7037(70)90009-8
- Sims, K. W. W., DePaolo, D. J., Murrell, M. T., Baldrige, W. S., Goldstein, S., Clague, D., & Jull, M. (1999). Porosity of the melting zone and variations in the solid mantle upwelling rate beneath hawaii: Inferences from u-238-th-230-ra-226 and u-235-pa-231 disequilibria. *Geochimica et Cosmochimica Acta*, 63(23–24), 4119–4138. doi: 10.1016/s0016-7037(99)00313-0
- Sims, K. W. W., Goldstein, S. J., Blichert-toft, J., Perfit, M. R., Kelemen, P., Fornari, D. J., et al. (2002). Chemical and isotopic constraints on the generation and transport of magma beneath the east pacific rise. *Geochimica et Cosmochimica Acta*, 66(19), 3481–3504. doi: 10.1016/s0016-7037(02)00909-2
- Spiegelman, M. (2000). Usercalc: A web-based uranium series calculator for magma migration problems. *Geochemistry, Geophysics, Geosystems*, 1(8), 1016. doi: 10.1029/1999gc000030
- Spiegelman, M., & Elliott, T. (1993). Consequences of melt transport for uranium series disequilibrium in young lavas. *Earth and Planetary Science Letters*, 118(1–4), 1–20. doi: 10.1016/0012-821x(93)90155-3
- Spiegelman, M., & Kenyon, P. (1992). The requirements for chemical disequilibrium during magma migration. *Earth and Planetary Science Letters*, 109(3–4), 611–620. doi: 10.1016/0012-821x(92)90119-g
- Stracke, A., & Bourdon, B. (2009). The importance of melt extraction for tracing mantle heterogeneities. *Geochimica et Cosmochimica Acta*, 73, 218–238. doi: 10.1016/j.gca.2008.10.015
- Stracke, A., Zindler, A., Salters, V. J. M., McKenzie, D., & Gronvold, K. (2003). The dynamics of melting beneath theistareykir, northern iceland. *Geochemistry, Geophysics, Geosystems*, 4, 8513. doi: 10.1029/2002gc000347
- Van Orman, J. A., Grove, T. L., & Shimizu, N. (2002). Diffusive fractionation of trace elements during production and transport of melting in the earth’s upper mantle. *Earth and Planetary Science Letters*, 198, 93–112. doi: 10.1016/s0012-821x(02)00492-2
- Van Orman, J. A., Saal, A. E., Bourdon, B., & Hauri, E. H. (2006). Diffusive fractionation of u-series radionuclides during mantle melting and shallow-level melt–cumulate interaction. *Geochimica et Cosmochimica Acta*, 70(18), 4797–4812.

- doi: 10.1016/j.gca.2006.07.005
- Yang, Z., Sista, S., Elmer, J. W., & DebRoy, T. (2000). Three dimensional monte carlo simulation of grain growth during gta welding of titanium. *Acta Materialia*, 48(20), 4813–4825. doi: 10.1016/s1359-6454(00)00279-2
- Zou, H., & Zindler, A. (2000). Theoretical studies of ^{238}u - ^{230}th - ^{226}ra and ^{235}u - ^{231}pa disequilibria in young lavas produced by mantle melting. *Geochimica et Cosmochimica Acta*, 64(10), 1809–1817. doi: 10.1016/s0016-7037(00)00350-1